Endothelial cell signature in muscle stem cells showed by VEGFA-FLT1-AKT1 axis for muscle stem cell survival

Authors/Affiliations

Mayank Verma[a,b,c,d], Yoko Asakura[b,c,d], Xuerui Wang[b,c,d], Kasey Zhou[b,c,d], Mahmut Ünverdi[b,c,d], Allison P. Kann[e,f], Robert S. Kraus[e,f] and Atsushi Asakura[b,c,d]

Department of Pediatrics & Neurology, Division of Pediatric Neurology, The University of Texas Southwestern Medical Center, TX, USA[a].

Stem Cell Institute[b], Paul & Sheila Wellstone Muscular Dystrophy Center[c], Department of Neurology[d], University of Minnesota Medical School, MN, USA

Department of Cell, Developmental, and Regenerative Biology[e], and Graduate School of Biomedical Sciences[f], Icahn School of Medicine at Mount Sinai, NY, USA.

Conflict of Interest

MV and AA are listed as inventors on a patent for anti-FLT1 antibody mediated therapy for DMD. AA received consulting fees from ShireHGT.

Abstract

Endothelial and skeletal muscle lineages arise from common embryonic progenitors. Despite their shared developmental origin, adult endothelial cells (ECs) and muscle stem cells (MuSCs) (satellite cells) have been thought to possess distinct gene signatures and signaling pathways. Here we shift this paradigm by uncovering how adult MuSC behavior is affected by the expression of a subset of EC transcripts. We used several computational analyses including single-cell RNAseq to show that MuSCs express low levels of canonical EC markers. We demonstrate that MuSC survival is regulated by one such prototypic endothelial signaling pathway (VEGFA-FLT1). Using pharmacological and genetic gain- and loss-of-function studies, we identify the FLT1-AKT1 axis as the key effector underlying VEGFA-mediated regulation of MuSC survival. All together, our data support that the VEGFA-FLT1-AKT1 pathway promotes MuSC survival during muscle regeneration, and highlights how the minor expression of select transcripts is sufficient for affecting cell behavior.

36 **Introduction**

37 Skeletal muscle and endothelial cells (ECs) and their progenitors from the trunk and limbs are
38 derived from the somites during early developments. Previous works demonstrated the existence
39 of bipotent progenitors which express both Pax3 and FLK1 (Eichmann et al., 1993; Ema et al.,
40 2006; Esner et al., 2006; Kardon et al., 2002; Tozer et al., 2007). These bipotent progenitors
41 migrate into trunk and limb buds from ventrolateral region of the somites to generate MyoD(+)
42 myogenic cells followed by skeletal muscle and PECAM1(+) ECs followed by vasculatures
43 (Hutcheson and Kardon, 2009; Kardon et al., 2002; Lagha et al., 2009; Mayeuf-Louchart et al.,
44 2016, 2014). In addition, FLK1(+) cells give rise to myogenic cells during development and
45 oncologic transformation (Drummond and Hatley, 2018; Mayeuf-Louchart et al., 2014; Motoike
46 et al., 2003). Lastly, multipotent mesoangioblasts, vessel-associated stem cells, have been
47 identified in embryonic dorsal aorta (Minasi et al., 2002). These cells are able to differentiate
48 into several types of mesodermal tissues including skeletal muscle and ECs (Roobrouck et al.,
49 2011). Interestingly, these myogenic cells show the same morphology as muscle satellite cells
50 (MuSCs), stem cell populations for skeletal muscle, and express a number of myogenic and EC
51 markers such as MyoD, M-cadherin, FLK1 and VE-cadherin (De Angelis et al., 1999). However,
52 it is not clear whether adult MuSCs derived from these bipotent progenitors still maintain
53 canonical EC signals. Curiously, blood vessel-associated myoendothelial cell progenitors that
54 express both myogenic and EC markers, and are able to differentiate into myogenic cells
55 following transplantation have been identified in the interstitial spaces of both murine and human
56 adult skeletal muscle (Tamaki et al., 2002; Zheng et al., 2007; Huang et al., 2014). However, the
57 relationship between these myoendothelial cell progenitors and MuSCs remains unclear.

58

59 Vascular endothelial growth factor (VEGF), specifically VEGFA modulates many
60 biological aspects including angiogenesis through its two receptors, FLT1 and FLK1. Although
61 FLK1 possesses stronger signaling capability and the major signaling receptor tyrosine kinase
62 (RTK) for VEGFA, FLT1 has considerably higher affinity for VEGF but weaker cytoplasmic
63 signaling capability. In normal tissue, FLT1 acts as a decoy receptor and a sink trap for VEGF
64 thereby preventing excessive normal and pathological angiogenesis. In addition, there are two
65 co-receptors for VEGFA (NRP1 and NRP2) that function with FLK1 to modulate VEGFA
66 signaling. While VEGF signaling has been extensively studied for its role in development,
67 proliferation, and survival of endothelial cells (ECs), its role in non-vascular systems such as
68 neuron and bone has only recently been appreciated (Liu et al., 2012; Okabe et al., 2014; Poesen
69 et al., 2008). Skeletal muscle tissue is the most abundant producer of VEGFA in the body. It has
70 already been extensively studied in the skeletal muscle fibers in models of *Vegfa* knockout mice
71 (Olfert et al., 2009; Tang et al., 2004; Wagner et al., 2006) as well as *Vegfa* overexpression
72 (Arsic et al., 2004; Bouchentouf et al., 2008; Messina et al., 2007; Yan et al., 2005).
73 Adult skeletal muscle also contains the tissue resident muscle stem cell population,
74 termed MuSCs, which mediate postnatal muscle growth and muscle regeneration (Motohashi and
75 Asakura, 2014). After muscle injury, quiescent MuSCs initiate proliferation to produce myogenic
76 precursor cells, or myoblasts. The myoblasts undergo multiple rounds of cell division before
77 terminal differentiation and formation of multinucleated myotubes by cell fusion. Importantly,
78 the MuSC-derived myoblasts also express VEGFA, which has been shown to increase the
79 proliferation of myoblasts (Christov et al., 2007). Our data obtained from genetical model mice
80 demonstrated that MuSCs express abundant VEGFA, which recruits ECs to establish vascular
81 niche for MuSC self-renewal and maintenance (Verma et al., 2018). In addition, VEGFA and its

82 receptors are expressed in the myoblast cell line, C2C12 cells, and the signaling can induce cell
83 migration and protect apoptotic cell during myogenic differentiation *in vitro* (Bryan et al., 2008;
84 Germani et al., 2003; Mercatelli et al., 2010). However, it is not clear whether MuSCs also
85 express VEGF receptors and if cell-autonomous VEGFA signaling plays an essential roles in
86 MuSC fucction during muscle regeneration *in vivo*.

87 We have previously shown that *Flt1* heterozygous gene knockout and conditional
88 deletion of *Flt1* in ECs display increased capillary density in skeletal muscle, indicating the
89 essential roles for *Flt1* in adult skeletal muscle. More importantly, when crossed with the
90 Duchenne muscular dystrophy (DMD) model *mdx* mice, these mice show both histological and
91 functional improvements of their dystrophic phenotypes. This was due to the effect of increased
92 ECs leading to an increase in MuSCs (Verma et al., 2010; Verma et al., 2019). However, the
93 effect of VEGFA on MuSC *in vivo* remained unknown. We found that MuSCs express low levels
94 of canonical EC markers including VEGF receptors using single cell transcriptomics. Therefore,
95 we examined the effects of VEGFA on MuSCs and show that it has a drastic effect on cell
96 survival in the via its receptor FLT1 by signaling through AKT1.

97

98 **Results**

99 **EC gene signal including *Vegf receptors* in MuSCs**

100 EC signatures in MuSCs has been seen in several gene expression data sets (Figure S1A-D,
101 Table S1) (Fukada et al., 2007; Ryall et al., 2015; van Velthoven et al., 2017; Yue et al., 2020).
102 However, with the lack of EC control, we questioned whether these were true expression or
103 artifact. To isolate EC and MuSC populations, we first crossed the $Flk1^{+/GFP}$ mice to label the
104 ECs of the vasculature (Ema et al., 2006) and the $Pax7^{+/CreERT2}$:$ROSO26^{+/Loxp\text{-}stop\text{-}Loxp\text{-}tdTomato}$

105 (*Pax7*$^{+/CreERT2}$:*R26R*$^{+/tdT}$) mice to mark the MuSC lineage (Murphy et al., 2011; Verma et al.,
106 2018). We performed bulk RNA sequencing (RNAseq) on FACS sorted ECs and MuSCs as well
107 as freshly isolated single muscle fibers (Figure 1A, S1E-G). We found that single muscle fibers
108 routinely have ECs fragments attached to the fiber (Figure S1G) and so we removed such fibers
109 based of Flk1^{GFP} expression from the samples collected for sequencing. We surveyed for
110 canonical genes for each cell type (Figure 1B) and found minimal but reliable expression of
111 canonical ECs genes such as *Pecam1*, *Cdh5*, *Kdr*, and *Flt1* in MuSCs.

112 It is possible that these EC signatures detecting in MuSCs were not due to small amounts
113 of contaminating ECs with very high expression of the canonical EC genes skewing the average
114 expression in MuSC RNA samples. To rule out this possibility, we performed single cell
115 RNAseq (scRNAseq) on MuSCs and ECs isolated from mouse hind limb muscle from both basal
116 condition and 3-days post injury to look at both quiescent and activated MuSCs from the reporter
117 mice specified above (Figure 1A). We could reliably delineate injured and activated MuSCs via
118 side and forward scatter (Figure S1H, S1I). We FACS isolated cells from both days separately
119 and spiked in 20% of the ECs into the MuSCs, and performed scRNAseq for each time point
120 (Figure 1A). We performed sequencing with ~300K read/cell compared with the commonly used
121 sequencing with 60K reads/cell, in order to maximize the possibility of detecting low abundance
122 transcripts (Zhang et al., 2020). In the aggregated dataset, the MuSCs showed low overlap
123 between D0 and D3 owing to the different stages of the myogenic differentiation cycle, while the
124 ECs clusters showed near perfect overlap (Figure 1C, 1D). While drastic morphological changes
125 in ECs have been shown during muscle regeneration (Hardy et al., 2016), transcriptomic changes
126 are much more tapered, especially compared with MuSCs (Latroche et al., 2017). We were able
127 to deconvolve the quiescent MuSCs from the activated and differentiating MuSCs, ECs, and

128 other cell types from gene signatures. (Figure S1J). We also introduced an artificial chromosome
129 loci in our sequencing reference genome to allow for mapping of custom genes such as *eGFP-*
130 *SV40* and *tdTomato-WPRE-BGHPolyA* transgenes and were able to confirm high expression of
131 these genes to their respective clusters (Figure 1E). Importantly, data from scRNAseq were able
132 to recapitulate the minimal expression of canonical EC genes in the MuSC clusters such as *Cdh5*
133 (Figure 1E) as seen in our Bulk RNAseq results (Figure 1B). These included the *Vegf receptors*
134 *Flk1* (*Kdr*) and *Flt1* (Figure 1E). As a quality control measure, we mapped parts of the three
135 transgene genes, *eGFP* from $Flk1^{+/GFP}$, and *tdTomato* and *CreERT2* from $Pax7^{+/CreERT2}$:$R26R^{+/tdT}$
136 that can be detected in ECs and MuSCs, respectively, as expected (Figure S1K).

137 Surprisingly, we also found *eGFP* in the MuSCs and *tdTomato* in EC fraction, while the
138 *CreERT2* expression remained mainly restricted to the MuSCs (Figure S1K). FACS analysis and
139 FACS-sorted cells confirmed that GFP(+) and tdTomato(+) cells are exclusively restricted as
140 ECs and MuSCs, respectively (Figure S1E, S1F). Therefore, we hypothesized that this was due
141 to the ambient free mRNA from the digested cells that is intrinsic to any droplet based single cell
142 sequencing platform. By using SoupX (Young and Behjati, 2018), we performed careful
143 background subtraction using genes expressed exclusively in myofibers as our negative control
144 and genes validated by *in situ* hybridization as a positive control (Figure S1K) (Kann and Krauss,
145 2019). We observed decreased but sustained *eGFP* expression in the MuSC fraction and
146 *tdTomato* expression in the EC fraction after SoupX subtraction (Figure S1K). In addition, the
147 EC signatures such as *Cdh5* expression in the MuSC fraction was also sustained. These results
148 conclude that MuSCs contain mRNAs from canonical ECs genes. We showed that the canonical
149 EC genes were broadly expressed in the myogenic cells in our dataset (Figure 1E).

150 Since detection of rare subpopulation in single cell dataset is a factor of cell numbers, we
151 re-analyzed previously published dataset with 2,232 myogenic cells across different states (Torre
152 et al., 2018; De Micheli et al., 2020). We were able to classify cell as quiescent, proliferative vs.
153 differentiating states based on the expression of *Calcr*, *Cdk1* and *Myog*, respectively (Figure
154 S1L). We noticed that EC prototypic markers such as *Flt1* are broadly expressed with small
155 amounts in MuSCs. Complementary data from different laboratories showed the clear expression
156 of EC prototypic markers such as *Cdh5*, *Flt1* and *Kdr*, using microarrays and Bulk-RNAseq
157 (Figure S1A, S1B; Fukada et al., 2007; Ryall et al., 2015). Recently, RNAseq data from fixed
158 quiescent, early activated and late activated MuSCs show that *Flt1* may be transiently
159 upregulated during the early activation process (Figure S1C) (Yue et al., 2020). To confirm
160 whether the EC gene mRNAs were transcribed from MuSCs, we utilized previously published
161 MuSC nascent RNA transcriptome from TU-tagged samples (Gay et al., 2013; van Velthoven et
162 al., 2017). As expected, *Myh1* was represented in the whole muscle but was absent in the TU-
163 tagged MuSCs (Figure 1F), indicating that the nascent MuSCs were devoid of cellular
164 contamination from other cells in the muscle. Inversely, the nascent MuSC transcript was over-
165 represented for MuSC related genes such as *Calcr* and *Sdc4*. Interestingly, we were able to detect
166 EC genes such as *Kdr* and *Pecam1* in the TU-tagged MuSC samples indicating that they were
167 actively transcribed by MuSCs (Figures 1F, S1D).

168 We also verified the expression of *Vegfr* genes (*Kdr*, *Flt1*, *Nrp1* and *Nrp2*) in MuSCs
169 using RT-qPCR (Figure 1G). In addition, we verified the expression of *Flt1* by performing *in-*
170 *situ* hybridization using RNAScope on MuSC on whole muscle fiber, which we currently believe
171 to be the gold standard for expression studies (Figure 1H). Finally, in MuSC-derived myoblasts,
172 NRP1and NRP2 expression was detectable with comparable intensity compared with EC cell

173 line, while FLT1 expression was detectable with lower intensity compared with EC cell line
174 (Figure 1I). By contrast, PECAM1, VE-Cadherin and FLK1 expression, which was clearly
175 detected in EC cell line, was undetectable level in myoblasts. Taken together, these data indicate
176 that there are both transcripts of these EC canonical genes and EC canonical proteins in MuSCs.
177

178 **VEGFA induces proliferation and cell survival but not differentiation in myoblasts**

179 Since VEGFRs were expressed in MuSCs in small amounts and their ligand, VEGFA, was
180 highly expressed in MuSCs (Figure 2A; Verma et al., 2018), we wanted to investigate whether
181 there were any biological effects to induction by VEGFA. We found that treatment with VEGFA
182 could increase proliferation of MuSC-derived myoblasts at low dose but inhibit proliferation at
183 high dose of VEGFA, a phenomenon that has been previously described in ECs (Noren et al.,
184 2016)) (Figure S2A). We saw no effect on differentiation by VEGFA as evaluated by myosin
185 heavy chain (MyHC) staining, fusion index and RT-qPCR (Figure S2B, S2C, S2D). By contrast,
186 crystal violet staining showed that VEGFA could significantly increase survived cell number of
187 myoblasts following UV-mediated apoptotic cell death induction (Figure S2E, S2F). To
188 investigate apoptosis in detail, we optimized Annexin V assay following thapsigargin-mediated
189 endoplasmic reticulum (ER)-stress (Hirai et al., 2010) so that we could study deviation at ~ED50
190 while still performing experiments to remove the confounding variable to proliferation from the
191 experimental setup (Figure S2G and S2H). We had previously shown that MuSCs are the
192 predominant cells that secrete VEGFA in skeletal muscle (Figure 2A; Verma et al., 2018) and
193 while adding exogenous VEGFA did not improve cell survival, blocking VEGFA via a soluble
194 form of FLT1-FC increased the number of apoptotic and necrotic myoblasts *in vitro* (Figure 2C-
195 E).

196

197 **VEGFA-facilitated cell survival in MuSC-derived myoblasts is mediated through FLT1**

198 To characterize the VEGF receptor responsible for the anti-apoptotic effect of VEGFA on
199 MuSC-derived myoblasts, we used pharmacological inhibitors of the VEGF receptors (Figure
200 2F). We used blocking antibody for the VEGF receptors FLT1 (anti-FLT1 antibody), small
201 molecule inhibitors for FLK1 (SU4502 and ZM306416) and the FLK1 co-receptor NRP1
202 (EG00229) (Figure 2D). Surprisingly, inhibiting FLK1, the major signaling RTK for VEGFA,
203 had no effect on myoblasts survival (Figure 3E). By contrast, blocking FLT1 via blocking
204 antibody greatly decreased the survival of myoblasts following thapsigargin induction (Figure
205 3E). To confirm this interesting result using genetic tools, we obtained myoblasts with *Pax7-*
206 *CreER*-inducible deletion of *Flt1* mice ($Pax7^{+/CreER}$:$Flt1^{Loxp/Loxp}$ or *MuSC-*$Flt1^{\Delta/\Delta}$) and the control
207 mice ($Pax7^{+/+}$:$Flt1^{Loxp/Loxp}$). *In vitro* 4-OHT-mediated genetic deletion of *Flt1* (MuSC-$Flt1^{\Delta/\Delta}$)
208 resulted in down-regulation of *Flt1* RNA and FLT1 protein expression (Figure S2I, S2J), and
209 increased spontaneous cell death even without induction of apoptosis (Figure 2F). By contrast,
210 *Flt1* deletion did not affect cell proliferation assessed by EdU staining or myogenic
211 differentiation assessed by MyHC staining (Figure S2K-M). When apoptosis was induced, the
212 *MuSC-*$Flt1^{\Delta/\Delta}$ myoblasts had increased apoptosis that was not responsive to exogenous VEGFA
213 (Figure 2G).

214

215 **AKT signaling is involved in apoptosis of muscle stem cells.**

216 VEGFA signaling is mediated through Extracellular signal-Regulated Kinase (ERK), p38
217 Mitogen-Activated Protein Kinase (MAPK), and Protein kinase B (AKT). In ECs, VEGFA is
218 known to protect cells from apoptosis via AKT (Domigan et al., 2015; Lee et al., 2007).

219 However, it is not known whether VEGFA can similarly activate AKT in MuSC-derived
220 myoblasts. While the role of AKT has been explored in proliferation and differentiation in
221 myoblasts, its role in apoptosis has not been well characterized (Loiben et al., 2017). We
222 assessed for AKT activation via phosphorylated AKT (pAKT) in MuSC-derived myoblasts. We
223 found that exogenous VEGFA could induce AKT phosphorylation (pAKT) (Figure 2H, 2I). This
224 response was blunted in *MuSC-Flt1*$^{\Delta/\Delta}$ myoblasts and was no longer responsive to VEGFA
225 (Figure 2H, 2I). Lastly, we wanted to confirm that AKT activation could improve myoblast
226 survival. We infected lentiviral *E4ORF1* or *MyrAKT* vectors in myoblasts (Figure 2J), both of
227 which gene products have been shown to specifically activate AKT without activating ERK or
228 p38 (Kobayashi et al., 2010). We found that overexpression of either of these genes improved
229 cell survival compared with the control *in vitro* following induction of apoptosis via thapsagargin
230 (Figure 2J). These data establish FLT1-AKT as the cascade linking VEGFA to apoptosis in
231 MuSC-derived myoblasts during muscle regeneration (Figure 2K).
232
233 **VEGFA-FLT1 pathway protects MuSCs from apoptosis *in vivo***
234 Endogenous and exogenous VEGFA have been shown to regulate cell survival and protect ECs
235 from apoptosis *in vitro* (Gerber et al., 1998; Lee et al., 2007). To assess whether additional
236 VEGFA had an effect of MuSC behaviors *in vivo*, we used mice carrying the *VEGFA*$^{+/Hyper}$ allele
237 for injury-mediated tibialis anterior (TA) muscle regeneration following $BaCl_2$ injection (Figure
238 3A, 3B) (Miquerol et al., 1999). MuSC-derived myoblasts from *Pax7*$^{+/tdT}$*:VEGFA*$^{+/Hyper}$ mice
239 showed around 2.8 fold increased expression of *Vegfa* but not the *Vegfrs* compared with
240 myoblasts from wild-type mice (Figure S3A). Interestingly, while treatment with VEGFA alone
241 had no effect on apoptosis *in vitro*, the MuSCs from *Pax7*$^{+/tdT}$*:VEGFA*$^{+/Hyper}$ mice showed

242 decreased cell death in regenerating muscle by 1 day following $BaCl_2$ injection (Figure 3C).
243 Consequently, single muscle fibers from *Pax7*$^{+/tdT}$:*VEGFA*$^{+/Hyper}$ mice showed increased number
244 of MuSCs, compared with those from *Pax7*$^{+/tdT}$:*VEGFA*$^{+/+}$ mice by 28 days following $BaCl_2$
245 injection (Figure 3D). In addition, muscle regeneration was promoted in *VEGFA*$^{+/Hyper}$ mice in
246 the early and late muscle repair processes as judged by fiber diameter (Figures 3B, 3E, 3F, S3B-
247 D).

248 We then performed the reciprocal experiment to investigate the consequence of *Vegfa*
249 loss in MuSCs *in vivo*, and utilized MuSC-specific *Vegfa* knockout mice
250 (*Pax7*$^{+/CreER}$:*VEGFA*$^{Loxp/Loxp}$). We have previously shown that vasculature in the MuSC-
251 *VEGFA*$^{\Delta/\Delta}$ mouse muscle is perturbed and the proximity between the MuSC and EC is increased
252 (Verma et al., 2018). However, the functional consequences of this remained unknown. We
253 confirmed that clear downregulatin of VEGFA protein in MuSC-derived myoblasts isolated from
254 MuSC-*VEGFA*$^{\Delta/\Delta}$ mice (Figure S3E). We noticed that deletion of *Vegfa* in MuSCs in the *MuSC-*
255 *VEGFA*$^{\Delta/\Delta}$ mouse muscle led to an increase in the proportion of dead MuSCs following $BaCl_2$
256 injection (Figure 3G). Consequently, the number of MuSCs in the MuSC-*VEGFA*$^{\Delta/\Delta}$ muscle were
257 significantly reduced following recovery after injury (Figure 3H). There was no difference in the
258 MuSC numbers in MuSC-*VEGFA*$^{\Delta/\Delta}$ muscle at homeostasis. In addition, the muscle had a
259 regenerative defect as indicated by the shift in fiber size distribution and increased adipose
260 following muscle injury (Figure 3B, 3I, 3J, S3F-H). While a limitation of this experiment is that
261 the MuSC fusion into the fiber also deletes *Vegfa* from the fiber themselves, muscle fiber
262 specific deletion of *Vegfa* has not shown to have an effect on fiber size (Delavar et al., 2014).
263 These data indicate that cell intrinsic VEGFA improves cell survival of MuSCs and that loss of
264 MuSC-derived VEGFA results in reduced muscle regeneration.

265 Since FLT1 but not FLK1 was detected in MuSCs and MuSC-derived myoblasts, we
266 asked whether the *Flt1* had an effect on MuSC survival *in vivo,* we evaluated cell death in
267 MuSCs from *MuSC-Flt1*$^{\Delta/\Delta}$ mouse muscle. We induced muscle regeneration using $BaCl_2$ for 1
268 day and assessed for cell death in MuSCs. As seen *in vitro*, we found that loss of *Flt1* in MuSCs
269 (Figure S2I, S2J) resulted in increased cell death during early regeneration (Figure 3K).
270 Consequently, single muscle fibers from *MuSC-Flt1*$^{\Delta/\Delta}$ mice showed decreased number of
271 MuSCs, compared with those from *MuSC-Flt1*$^{+/+}$ mice by 28 days following $BaCl_2$ injection
272 (Figure 3L). We also examined the long-term *in vivo* consequence of deleting *Flt1* from MuSC.
273 There was no significant muscle phenotype in MuSC-*Flt1*$^{\Delta/\Delta}$ muscle at homeostasis (Figures 3B,
274 3M, 3N). However, following injury, the MuSC-*Flt1*$^{\Delta/\Delta}$ muscle had a modest regenerative defect
275 as indicated by the shift in fiber size distribution following muscle injury (Figures 3B, 3M, 3N,
276 S3J-N).
277
278 **VEGFA-FLT1 pathway regulates muscle pathology in DMD model mice**
279 While angiogenic defects have been reported in the *mdx* mice as well as in golden retrieval
280 muscular dystrophy (GRMD; canine model of DMD) (Latroche et al., 2015; Verma et al., 2019,
281 2010; Kodippili et al., 2021; Podkalicka et al., 2021), it is not clear whether VEGF family and its
282 receptors are implicated in human dystrophinopathies. We probed the VEGF ligands and
283 receptors in microarrays (Table S1) from skeletal muscles and MuSCs from *mdx* mice
284 (Pallafacchina et al., 2010; Tseng et al., 2002) and skeletal muscles from the *GRMD* (Vieira et al.,
285 2015). *Vegfa* was downregulated in both models (Figure S4A). *Flt1* was also downregulated in
286 *GRMD* but not *mdx* muscles. To examine whether VEGF signaling is altered in DMD patients,
287 we performed gene expression analysis on previously available data from microarrays from

288 patients with DMD (Chen et al., 2000). We also aggregated and probed microarray data from
289 muscle biopsies of patients with various neuromuscular diseases or of healthy individuals after
290 exercise (Bakay et al., 2006). In the microarray data, *Vegfa* expression was increased after an
291 acute bout of exercise, and *Vegfa* expression was reduced in ALS muscle, BMD muscle, as well
292 as both early and late phases of DMD muscle (Figure S4A). These data indicate that *Vegfa*
293 expression is decreased in dystrophinopathy, and thus may benefit people with DMD by
294 increasing VEGFA as a therapeutic target.

295 Therefore, we crossed the *MuSC-Flt1*$^{\Delta/\Delta}$ mice with the chronically regenerating DMD
296 model mice (*mdx*) to generate *mdx:MuSC-Flt1*$^{\Delta/\Delta}$ mice, and analyzed long term effects of *Flt1*
297 deletion (Figure 4A, S4B). Importantly, we found a significant decrease in fiber diameter and
298 increased fibrosis (Figures 4B-D, S4C) in TA muscle accompanied by a physiological decease in
299 muscle perfusion as shown by laser Doppler flow at 12 months age (Figure 4E) as well as a
300 functional decline in muscle strength as judged by grip strength both acutely and chronically
301 (Figure 4F).

302 By contrast, when we crossed the *VEGFA*$^{+/Hyper}$ mice with *mdx* mice (Figure 4A, S4D),
303 we noticed a significant increase in fiber diameter and decreased fibrosis (Figures 4G-I, S4E) in
304 both TA and diaphragm muscle of *mdx:VEGFA*$^{+/Hyper}$ mice accompanied by a physiological
305 increase in muscle perfusion as shown by laser Doppler flow at 12 months age (Figure 4J) as
306 well as a functional increase in muscle strength as judged by grip strength (Figure 4K). These
307 data indicate that VEGFA-FLT1 axis is a therapeutic target for the pathology seen in the *mdx*
308 mice

309

310 **Discussion**

311 In this report, we performed bulk and single cell RNA sequencing on MuSCs and ECs. Since
312 deep reads can significantly reduce the effect of the technical noise in scRNAseq, it can improve
313 estimation of minor transcriptional state of a given cell (Zhang, 2020). Unexpectedly, we found
314 that MuSCs broadly express EC prototypic markers in small amounts and used multiple different
315 bioinformatics techniques to validate the results. While similar phenomenon in myogenic cells
316 during development and existence of blood vessel-associated myoendothelial cells in the adult
317 skeletal muscle have been previously described, no functional follow up as been performed
318 leading to the questions whether these minor expression profiles were artifacts or functional (De
319 Angelis et al., 1999; Minasi, 2002; Tamaki et al., 2002; Zheng et al., 2007; Roobrouck, 2011;
320 Huang et al., 2014; Charville et al., 2015; Goel et al., 2017; Giordani et al., 2018). Our goal was
321 to see whether this small expression pattern had biological consequences. We ultimately decided
322 to use *Flt1* for further investigations and used RNAscope and immunostaining to validate its
323 expression in MuSCs. We found that *Flt1* indeed exerts a biological function even at a low
324 expression. Signaling through VEGFA-FLT1-AKT can improve cell survival in MuSCs both *in*
325 *vivo* and *in vitro.*

326 On a grander scale, our finding of EC prototype markers expressed in MuSC calls into
327 two questions 1) the genes that we used to specify cellular identities and 2) the cellular identity
328 of MuSCs and ECs. The former is important as when we experimentally label, induce or perform
329 Cre-mediated gene knockout experiments based on our assumptions of different gene expression
330 results which may be confounded for these low expressing genes. For example, we have
331 previously investigated both *Flt1* and *Kdr* in mouse muscle using three different reporters and

332 found them to be negative in MuSCs, thereby disregarding their cell-autonomous effect when
333 evaluating global knockouts (Verma et al., 2018, 2010). It is also possible that EC mRNAs are
334 results of transcription from the cell or a result of mRNA transfer from neighboring cells
335 (Desrochers et al., 2016). Of note, the transmission of *tdTomato* mRNA and protein from
336 *Pax7*$^{+/CreERT2}$*:R26R*$^{+/tdT}$ mice used in this study has been recently shown via exosome, opening
337 up the possibility of transmission of other mRNA from MuSC to ECs (Murach et al., 2020). The
338 later is an interesting phenomenon form a developmental point of view. MuSCs and ECs arise
339 from a bipotent progenitor originated from somites during early development (Kardon et al.,
340 2002; Hutcheson, 2009; Lagha, 2009; Mayeuf-Louchart, 2014; Mayeuf-Louchart, 2016).
341 Therefore, it is possible that there is a permissive chromatin state that allows for expression of
342 reciprocal genes in the two populations. Along the lines of these observations, FLK1(+) or VE-
343 cadherin(+) cells can contribute to myogenic cells *in vitro* and after cell transplantation (Tamaki
344 et al., 2002; Le Grand et al., 2004; Zheng et al., 2007; Huang et al., 2014;), and during
345 development (Drummond and Hatley, 2018; Mayeuf-Louchart et al., 2014; Motoike et al., 2003).
346 Important notion is that the PDGFRα(-)FLK1(+) population exhibited restricted potential to
347 differentiate into the MuSCs in injured muscle (Sakurai et al., 2008). Interestingly, in the
348 zebrafish, exogenous expression of *Etv2* in the fast muscle can lead to transdifferentiation of
349 muscle fibers into functional vessels so there is evidence of cell fate flexibility (Veldman et al.,
350 2013). The potential of EC transdifferentiation was also examined by ETV2 overexpression in
351 five human cell types, skeletal muscle cells, adipose-derived mesenchymal stem cells, umbilical
352 cord-derived mesenchymal stem cells, embryonic lung fibroblast cells and skin fibroblast cells.
353 Among them, human skeletal muscle cells showed the highest amenability for this EC induction
354 following infection with ETV2 lentivirus vector (Yan et al., 2019). Conversely, *Etv2*-deficient

355 vascular progenitors can differentiate into skeletal muscle cells (Chestnut et al., 2020). It would
356 be interesting to see whether other EC gene signatures also have functional consequences in the
357 MuSC or muscle at large.

358 We decided to focus on function of *Flt1* among several EC genes expressed in MuSCs
359 for further investigations on MuSC biology. Our pharmacological and genetic analyses
360 demonstrate that MuSC-derived VEGFA has a drastic effect on cell survival in the via its
361 receptor FLT1 by signaling through AKT1. While VEGFA binds to both FLT1 and FLK1,
362 VEGFB and PGF only bind to FLT1. This creates a scenario where PGF and VEGFB binding
363 can sequester FLT1, increasing free VEGFA availability for VEGFA-FLK1 binding which is the
364 major VEGF signaling pathway for many cell types (Vempati et al., 2014). While PGF is not
365 normally expressed in adult tissues, VEGFB is expressed in the MuSCs and muscle fiber (data
366 not shown). Importantly, the VEGFB-FLT1 axis has also been shown to inhibit apoptosis in
367 retina and brain cells in mouse models of ocular neurodegeneration and stroke (Li et al., 2008).
368 While our results cannot rule out the involvement of VEGFB in protection of MuSC apoptosis,
369 we provide evidence from both pharmacological and genetic data to indicate that VEGFA is
370 involved.

371 Despite drastic effect of VEGFA-FLT1 on apoptosis *in vitro*, the long-term consequences
372 of *in vivo* deletion of *Flt1* in the MuSC compartment were modest compared with deletion of
373 *Vegfa* in the MuSCs unless crossing with *mdx* mice. Although *Vegfa* is required for both MuSC
374 survival and recruitment of vascular niche (Verma et al., 2018), in the steady state, the MuSC
375 turnover may be low enough that the apoptotic stress burden is low. VEGFA improves cell
376 survival during the proliferative stage following injury, however this transient improvement in

377 survival has only a modest impact on the final regenerative process as shown in
378 *mdx:VEGFA*$^{+/Hyper}$ mice.

379 VEGFA and FLT1 targeted therapies are being explored as both pro- and anti-angiogenic
380 therapies for several indications including retinal degeneration, cancer, pre-eclampsia and
381 neuromuscular diseases (Bae et al., 2005; Keifer et al., 2014; Mac Gabhann et al., 2011; Verma
382 et al., 2010; Verma et al., 2019; Bosco et al., 2021; Xin et al., 2021). As these therapies mature,
383 it will be important to ascertain the MuSC-specific effects of VEGFA and FLT1.

384

385 **Materials and Methods**

386 **Mice**

387 *Flt1*$^{LoxP/LoxP}$ were obtained from Gua-Hua Fong (Ho et al., 2012). *B6.Cg-Pax7*$^{tm1(cre/ERT2)Gaka/J}$
388 (*Pax7*$^{+/CreERT2}$; JAX stock# 017763; Murphy et al., 2011), *B6.Cg-Gt(ROSA)*$^{26Sortm9(CAG-tdTomato)Hze/J}$
389 (*Ai9*; JAX stock # 007909; Madisen et al., 2010), *VEGFA*$^{+/Hyper}$ (*Vegfatm1.1Nagy/J*; JAX stock#
390 027314; Miquerol et al., 1999) and *B6Ros.Cg-Dmd*$^{mdx-5cv}$*/J* (*mdx*^{5cv}; JAX stock #002379;
391 Chapman et al., 1989) were obtained from Jackson Laboratory. *Kdr*$^{tm2.1Jrt/J}$ (*Flk1*$^{+/GFP}$) were
392 obtained from Masatsugu Ema (Ema et al., 2006). *B6.Cg-Pax7*$^{tm1(cre/ERT2)Gaka/J}$ (*Pax7*$^{+/CreERT2}$)
393 mice were crossed with the *B6.Cg-Gt(ROSA)*$^{26Sortm9(CAG-tdTomato)Hze/J}$ (*Ai9*) to yield the
394 *Pax7*$^{+/CreERT2}$*:R26R*^{tdT}(*Pax7*^{tdT}) mice. *Pax7*^{tdT} mice were bred with the *VEGFA*$^{+/Hyper}$ and
395 *Flk1*$^{+/GFP}$ to obtain *Pax7*$^{+/tdT}$:*VEGFA*$^{+/Hyper}$ and *Pax7*$^{+/tdT}$*:Flk1*$^{+/GFP}$ mice. *VEGFA*$^{LoxP/LoxP}$ mice
396 obtained from Napoleone Ferrara (Gerber et al., 1999) were crossed with *Pax7*$^{+/CreERT2}$ to yield
397 the *Pax7*$^{+/CreERT}$*: VEGFA*$^{LoxP/LoxP}$ mice. *Flt1*$^{LoxP/LoxP}$ mice obtained from Guo-Hua Fong (Ho et al.,
398 2012) were crossed with *Pax7*$^{+/CreERT2}$ to yield the *Pax7*$^{+/CreERT}$*:Flt1*$^{LoxP/LoxP}$ mice. Colonies for all
399 the mice were established in the laboratory. Cre recombination was induced using tamoxifen
400 (Sigma-Aldrich, T5648) dosed as 75 mg/kg body weight x 3 times over one week at 3-6 weeks
401 of age. Mice carrying the wild-type *CreERT2* allele were used for control experiments. TA
402 muscle regeneration was induced by intramuscular injection of 20 µl of 1% $BaCl_2$ (Sigma-
403 Aldrich, 342920) or 20 µl of 10 µM Cardiotoxin (CTX) (Sigma-Aldrich, V9125). Mice used for
404 this study is summeried in Table S2.

405 Genotyping to detect the transgenic and mutant alleles was performed by PCR using the
406 primers described on the web site of Jackson Laboratory shown in Table S3. All primers were
407 synthesized as custom DNA oligos from Integrated DNA technologies (IDT). Genotyping to

408 detect the mutated allele of *mdx*^{5cv} was performed by PCR using the primers (0981 and 0982)
409 shown in Table S1. The PCR product DNA was digested with *Dra*III restriction enzyme (New
410 England Biolabs, R3510S). Wild-type allele generated 180 bp and mutant allele generated 50
411 and 130 bp bands.

412 The animals were housed in an SPF environment and were monitored by the Research
413 Animal Resources (RAR) of the University of Minnesota. All protocols were approved by the
414 Institutional Animal Care and Usage Committee (IACUC) of the University of Minnesota and
415 complied with the NIH guidelines for the use of animals in research.

416

417 **Cell isolation by FACS**

418 *Pax7*^{tdT}*:Flk1*^{GFP} mice were utilized for FACS-mediated MuSC and EC isolation as previously
419 described (Asakura et al, 2002; Verma, 2018). We performed extensive validation of the
420 fluorescent reporter mice as previously described (Figure S1A-C; Verma, 2018). Briefly,
421 quiescnet MuSCs and ECs were isolated from the hind limb skeletal muscle of 1–2-mo-old
422 *Pax7*^{tdT}*:Flk1*^{GFP} mice after digestion with collagenase type II. FACS was performed on an FACS
423 sorter (BD FACSAria) and data were analyzed using FlowJo (BD Biosciences). Sorting gates,
424 tdTomato(+) for MuSCs and GFP(+) for ECs, were strictly defined based on control cells
425 isolated from wild-type mice and the forward scatter and side scatter gating. Sorted cells were
426 immediately characterized by immunostaining on slide glasses, utilzed for RNA preparation or
427 cultured on collagen-coated plates in the myoblast growth medium as below to obtain MuSC-
428 derived myoblasts and ECs. FACS analysis was performed as previously described (Turaç et al.,
429 2013). Cells were either trypsinized (cultured cells) or a single cell suspension was obtained
430 following enzymatic digestion as whole muscle-derived cells (Asakura, 2002). Cells were then

431 washed with FACS buffer (2% BSA and 1 mM EDTA in PBS) followed by live/dead staining
432 using ZombieNIR (Biolegends, 423105). Cells were washed, then immunostained for cell
433 surface markers. Blocking cells was performed with 1% BSA/PBS, and cells were incubated in
434 fluorescently-conjugated antibody. FACS was performed on a Fortessa X-20 (BD Biosciences)
435 with a 355 nm, 405 nm, 488 nm, 561 nm, and 640 nm lasers.
436
437 **Cell culture**
438 MuSC-derived myoblast isolation from adult mice was performed as previously described
439 (Asakura et al, 2001; Motohashi et al., 2014). Briefly, after collagenase type II (Worthington,
440 CLS-2) treatment, dissociated cells from mouse hindlimb muscle were incubated with anti-
441 CD31-PE (eBiosciences, 12-0311), anti-CD45-PE (eBiosciences, 30-F11), anti-Sca1-PE
442 (eBiosciences, Dec-81) and anti-Integrin α7 (MBL International, ABIN487462), followed by
443 anti-PE microbeads (Miltenyi Biotec, 130-048-801), and then performed LD column (Miltenyi
444 Biotec, 130-042-901) separation. Negative cell populations will be incubated with anti-Mouse
445 IgG beads (Miltenyi Biotec, 130-048-402), and then MS coulumn (Miltenyi Biotec, 130-042-
446 201) separation was performed to isolate Integrin α7(+) MuSCs. MuSC-derived myoblasts were
447 maintained in culture on collagen coated plates in myoblast medium containing 20% FBS and 20
448 ng/ml bFGF (Invitrogen, PHG0263) in HAM's-F10 medium. Cell cultures were maintained in a
449 humidified incubator at 37°C with 5% CO_2 and 5% O_2. 4-hydroxy tamoxifen (4-OHT, Sigma-
450 Aldrich, H6278) treatment (1 μM in EtOH) was used to induce *Flt1* deletion in myoblasts
451 isolated from $Flt1^{LoxP/LoxP}$:$Pax7^{CreERT2}$ mice. For cell survival assay, 1 x 10^5 cells were allowed to
452 adhere for one day and starved overnight in 0.1% FBS in HAM's F10 medium. Then, cells were
453 exposed to 1 μM EdU along with or withpout 2-100 ng/ml recombinant VEGFA (R&D Systems,

454 493-MV) for 8 hours before being fixed and stained by the Click-iT EdU Alexa Fluor 488
455 Imaging Kit (Thermo Scientific, C10337). For induction of apoptosis in myoblasts, (1-2 x 10^5)
456 cells were allowed to adhere to the plates for 16 hours. Thapsigargin-mediated apoptosis was
457 induced by 1 μM of thapsigargin (Sigma-Aldrich, T9033) dissolved in EtOH with or without
458 VEGFA, 100 ng/ml recombinant FLT1-FC (R&D Systems, 7756-FL), 1 μg/ml anti-FLT1
459 monoclonal antibody (Angio-Proteomie, MAB7072), inhibitors of FLK1, 3 μM ZM306416
460 (R&D Systems, 2499/1) and 10 μM of SU5402 (R&D Systems, 3300/1) and an inhibitor of
461 NRP1, 30 μM of EG00229 (R&D Systems, 6986/10) for 24 hours. UV light-mediated apoptosis
462 was induced by exposing the cells to UV light in cell culture hood for 45 seconds without
463 medium. After UV exposure, cell survival was assessed 24 hours following culture in 0.1% FBS
464 in HAM's F10 medium with or without VEGFA using the Crystal violet Assay Kit (Abcam,
465 ab232855) and quantated the Crystal violet dye after solubilization by absorbance at 570 nm. To
466 induce differentiation of myoblasts, the myoblast medium was replaced with differentiation
467 medium that contained DMEM supplemented with 5% horse serum with or withour VEGFA or
468 bFGF for 1 or 3 days followed by anti-sarcomeric myosin heavy chain antibody (Developmental
469 Study Hybridoma Bank, MF-20).
470
471 **AKT induction**
472 The lentiviral pCCL-E4ORF1 and pCCL-myrAkt1 constructs were a kind gift from Dr. Jason
473 Butler (Kobayashi et al., 2010). 293FT cells (Thermo Fisher Scientific, R70007) were seeded in
474 DMEM with 10% FBS and transfected with the lentivirus vectors along with pCMV-VSV-G
475 (Addgene, 8454), pRSV-Rev (Addgene, 12253), and pMDLg/pRRE (Addgene, 12251) using
476 PolyJet transfection reagent (Signagen Laboratories, SL100688). The culture supernatant of the

477 transfected 293FT cells was added to MuSC-derived myoblast culture with 0.8 μg/ml polybrene
478 (MilliporeSigma, H9268). pAKT1(+) cells were stainined with anti-pAKT antibody (Cell
479 Signaling, 4060).
480
481 **Apoptosis assay**
482 Apoptosis was measured using measured using Annexin V-Biotin Apoptosis Detection Kit
483 (eBioscience™, BMS500BT-100) as per the manufacture's instruction. Streptavidin-conjugated
484 AlexaFluro-488 was used for detection. Propidium Iodide (PI) was used in all assays except
485 when Pax7tdT(+) cells were utilized or when ZombieNIR (Biolegends, 423105) was used. FACS
486 was performed on a Fortessa X-20 (BD Biosciences) equipped with a 355 nm, 405 nm, 488 nm,
487 561 nm, and 640 nm lasers.
488
489 **Immunostaining of cells**
490 Immunostaining for PECAM1, VE-Cadherin, VEGFA, VEGFRs was performed on collagen
491 coated coverslips. Other immunostaining was performed on 30 mm tissue culture plates. Cells
492 were fixed with 2% PFA for 5 minutes and immunostained as previously described (Verma et al.,
493 2010). For membrane receptor staining, cells were permeabilized with 0.01% saponin
494 (ThermoFisher Scientific, ICN10285525) which was kept in the staining solution until the
495 primary antibodies were washed off. At which time, 0.01% Triton-X was added to all the buffers.
496 The antibodies used for this study are listed in Table S4.
497
498 **Single muscle fiber isolation and staining**

499 Extensor digitorum longus (EDL) muscle was dissected and digested with 0.2% collagenase type
500 I (Sigma-Aldrich, C0130) for single muscle fiber isolation as previously described (Verma et al.,
501 2010). Single muscle fibers were fixed with 2% PFA/PBS, permeabilized with 0.2% Triton-
502 X100 and counterstained with DAPI. Anti-Pax7 antibody(+) or tdTomato(+) MuSCs per single
503 muscle fiber were counted manually.
504
505 **RNAscope**
506 RNAscope for *Flt1* transcripts was performed as previously described (Kann and Krauss, 2019)
507 on single muscle fibers from $Pax7^{tdT}$ mice using the RNAscope Probe - Mm-Flt1 (C1) (ACDBio,
508 415541). Briefly, isolated EDL fibers are fixed in 4% PFA, washed with PBS, and dehydrated in
509 100% methanol. Subsequently, fibers are rehydrated in a stepwise gradient of decreasing
510 methanol concentrations in PBS/0.1% Tween-20. Fibers are treated with a proteinase for 10
511 minutes, followed by hybridization, amplification, and fluorophore conjugation steps.
512
513 **Histology**
514 The mouse tibialis anterior (TA) muscle was used for all histological analysis. Tissues were
515 frozen fresh using LiN_2 chilled isopentane and stored at -80ºC. Eight µm thick transverse
516 cryosections were used for all histological analysis. Hematoxylin & Eosin (HE) staining were
517 performed as previously described (Verma et al., 2010). Sirius red (Direct Red 80, Sigma-
518 Aldrich, 365548) staining was performed for muscle sections for fibrosis as previously described
519 (Shimizu-Motohashi et al., 2015). Muscle sections were stained in Oil Red O solution (Sigma-
520 Aldrich, O1391-250ML) as previously described (Wang et al., 2017). Microscopic images were
521 captured by a DP-1 digital camera attached to BX51 fluorescence microscope with 10x or 40×

522 UPlanFLN objectives with cellSens Entry 1.11 (all from Olympus). Photoshop (Adobe) and Fiji
523 (NIH) were used for image processing and manually enumerating the fiber diameter (Schindelin
524 et al., 2012).
525
526 **Grip strength test**
527 Forelimb grip strength test was performed following a previously published procedure (Aartsma-
528 Rus and van Putten, 2014). Briefly, mice were gently pulled by the tail after fore limb-grasping a
529 metal bar attached to a force transducer (Grip Strength Meter, Columbus Instruments, 1027CSM-
530 D52). Grip strength tests were performed by the same blinded examiner. Five consecutive grip
531 strength tests were recorded, and then mice were returned to the cage for a resting period of 20
532 minutes. Then, three series of pulls were performed each followed by 20 min resting period. The
533 average of the three highest values out of the 15 values collected was normalized to the body
534 weight for comparison.
535
536 **Muscle perfusion**
537 RBC flux was evaluated using the moorLabTM laser Doppler flow meter as previously described
538 (Verma, 2010) with the MP7a probe that allows for collecting light from a deeper tissue level
539 than standard probes according to the manufacturer's instructions (Moor Instruments). The fur
540 from the right hind leg was removed using a chemical depilatory. Readings were taken using the
541 probe from at least 10 different spots on the TA muscle. The AU was determined as the average
542 AU value during a plateau phase of each measurement.
543
544 **RNA and genomic DNA isolation and qPCR**

545 Cultured cells were washed with ice cold PBS and lysed on the place with Trizol™. RNA was
546 isolated using the DirectZol™ RNA Microprep Kit (Zymo Research, R2062) with on-column
547 DNase digestion followed by cDNA synthesis using the Transcriptor First Strand cDNA
548 synthesis kit (Roche Molecular Diagnostics, 04379012001) using random primers. Genomic
549 DNA for genotyping was isolated from mouse tail snips with lysis buffer containing Proteinase
550 K (Sigma-Aldrich, P2308). qPCR was performed using GoTaq qPCR Master Mix (Promega,
551 A6002). The input RNA amount was normalized across all samples and *18S rRNA* or *HtatsF1*
552 was used for normalization of qPCR across samples. Primer sequences are listed in Table S3. All
553 primers were synthesized as custom DNA oligos from Integrated DNA technologies (IDT).
554

555 **Single cell RNAsequencing and analysis**

556 Cells for single cell RNAseq were obtained from hind limb muscles of 2-3 moth-old
557 *Pax7^{tdT}:Flk1^{GFP}* mice following enzymatic digestion as previously described (Liu et al., 2015).
558 Dead cells were excluded from the analysis using ZombieNIR (Biolegends, 423105).
559 TdTomato(+) and GFP(+) cells were sorted individually and then 20% of GFP(+) cells were
560 spiked into 80% tdTomato(+). We loaded ~5,000 cells into 1 channel of the Chromium system
561 for each of these samples and prepared libraries according to the manufacturer's protocol using
562 version 2.0 chemistry (10x Genomics). Following capture and lysis, we synthesized cDNA and
563 amplified for 12 cycles as per the manufacturer's protocol (10x Genomics). The amplified cDNA
564 was used to construct Illumina sequencing libraries that were each sequenced with ~300K
565 read/cell on one lane of an Illumina HiSeq 2500 machine. We used Cell Ranger 3.1 (10X
566 Genomics) to process raw sequencing data. For A custom genome was constructed to include
567 *eGFP-SV40*, *tdTomato-WPRE-BGHPolyA* and *Pax7-IRES-CreERT2* transgenes. Detailed step-

568 by-step instructions can be found at https://github.com/verma014/10XCustomRef. We carried
569 out analyses of the filtered data using Seurat suite version 3.0 (Stuart et al., 2019) in R studio
570 (RStudio Team, 2020). For cell imputation, we utilized ALRA through the Seurat wrapper with
571 default settings(Linderman et al., 2018). Additional scRNAseq datasets were obtained from GEO
572 and analyzed using the same method as listed above. A myogenic score was calculated based on
573 the expression of *Myog*, *Pax7*, *Myod1* and *Myf5*. Step-by-step instructions for the analysis can be
574 found on https://github.com/verma014/10XCustomRef.
575
576 **Background Subtraction**
577 10x Genomics scRNAseq platform uses many more droplets than cells and so following a run,
578 there are many droplets that do not have cells. These droplets still get sequenced with some of
579 the RNA that is in the solution. This floating RNA can be used to estimate the "background" in
580 each droplet. A better description of this can be found by the developers of 'SoupX' (Young and
581 Behjati, 2020). Since *Cdh5* expression has previously been verified in MuSCs using RNAscope,
582 we were able to use it as a positive control to remove the background or "soup" from our data. If
583 *Cdh5* is absent from MuSC, we know that the background subtraction was too aggressive and
584 that subtracting the Soup is not reliable in our case. In addition, we know certain genes that are
585 considered to be specific for MuSCs, muscle ECs or muscle fibers based on the bulk RNAseq
586 (Verma et al., 2018). The top 5 genes that are specific to these population (and also detected by
587 10x) were selected and used to show the background in our data set was 14.40% and 13.89% for
588 the D0 and D3 dataset, respectively. The step-by-step instructions can be found on
589 https://github.com/verma014/10XCustomRef.
590

591 **Bulk RNAseq and Microarray Analysis**

592 FASTQ files were downloaded from SRA using SRA-toolkit. Sequences were trimmed using
593 trimmomatic to remove adapter contamination and low-quality reads. Trimmed sequences were
594 mapped to mouse mm10 using Hisat2 (Pertea et al., 2016). Transcript assembly was performed
595 using StringTie (Pertea et al., 2016). Cell type specificity was determined as previously
596 described (Verma et al., 2018). Microarray analysis was performed using the Affymetrix
597 Transcriptome Analysis Console (TAC). Samples in each experiment were RNA normalized and
598 the expression was acquired using the Affeymetrix Expression analysis console with gene level
599 expression. Heatmaps were generated in Prism 9 (Graphpad, La Jolla, CA). The code for
600 generating each graph is listed in the following table, along with the link to the data in tabular
601 format.

602

603 **Quantification and Statistical Analysis**

604 Statistical analysis was performed using Prism 9 (Graphpad, La Jolla, CA) or RStudio (RStudio
605 Team, 2020). For comparison between two groups, an unpaired T-test was used. For comparison
606 between multiple groups, a one-way ANOVA was used with multiple comparisons to the control.
607 Distributions were compared using a chi-squared test. Graphing of the data was performed using
608 Prism 9. Vector diagrams were modified using Graphic (Autodesk). All values are means ±SEM
609 unless noted otherwise. * indicates $p < 0.05$, ** indicates $p < 0.01$, *** indicates $p < 0.001$.

610

611 **Data and Software Availability**

612 All the data was obtained from NCBI GEO. Microarrays of mouse MuSCs were obtained from
613 GSE3483 (Fukada et al., 2007). scRNAseq of MuSCs and muscle ECs was performed in this

study (GSE129057). scRNAseq of whole muscle was obtained from GSE143437 (De Micheli et al., 2020). Bulk RNAseq of MuSCs, ECs and single muscle fibers was obtained from GSE108739 (Verma et al., 2018) and GSE64379 (Ryall et al., 2015). Bulk RNAseq of TU-tagged RNA of MuSCs was obtianed from GSE97399 (van Velthoven et al., 2017). Bulk RNAseq of fixed and unfixed MuSCs was obtained from GSE113631 (Yue et al., 2020). Exercise, ALS, DMD, BMD, FSHD GSE3307, Early DMD GSE465, *mdx* GSE466, GRMD GSE69040, Satellite cells GSE15155. All arrays were normalized to their respective controls. All arrays and RNAseq data are listed in Supplemental Table 1 (Table S1).

Acknowledgements

We thank Minnesota Supercomputing Institute, University of Minnesota Imaging Center, University of Minnesota FACS Facility, and University of Minnesota Genomics Center for providing data for this paper. We also thank Jake Trask for critical reading of this paper. We thank Drs. Yosuke Mukouyama (National Institute of Health), Napoleone Ferrara (Genentech), Guo-Hua Fong (University of Connecticut) and Masatsugu Ema (Siga University of Medical Science) for providing *VEGFA*$^{LoxP/LoxP}$, *Flt1*$^{LoxP/LoxP}$ and *Flk1-GFP* mice, respectively. This work was supported by NIHT32-GM008244 and NIHF30AR066454 to MV and NIHR01AR062142, NIHR21AR070319, MDA Research Grant, and Regenerative Medicine Minnesota (RMM) Grant to AA.

Competing interests

The authors declare no competing interests.

637 **Reference**

638 Aartsma-Rus A, van Putten M. 2014. Assessing Functional Performance in the Mdx Mouse
639 Model. *J Vis Exp*. doi:10.3791/51303

640 Arsic N, Zacchigna S, Zentilin L, Ramirez-Correa G, Pattarini L, Salvi A, Sinagra G, Giacca M.
641 2004. Vascular endothelial growth factor stimulates skeletal muscle regeneration in vivo.
642 *Mol Ther* **10**:844–854. doi: 10.1016/j.ymthe.2004.08.007

643 Asakura A, Komaki M, Rudnicki M. 2001. Muscle satellite cells are multipotential stem cells
644 that exhibit myogenic, osteogenic, and adipogenic differentiation. *Differentiation* **68**:245–
645 253. doi: 10.1046/j.1432-0436.2001.680412.x.

646 Asakura A, Seale P, Girgis-Gabardo A, Rudnicki MA. 2002. Myogenic specification of side
647 population cells in skeletal muscle. *J Cell Biol* **159**:123–134. doi: 10.1083/jcb.200202092.

648 Bae DG, Kim TD, Li G, Yoon WH, Chae CB. 2005. Anti-flt1 peptide, a vascular endothelial
649 growth factor receptor 1-specific hexapeptide, inhibits tumor growth and metastasis. *Clin*
650 *Cancer Res* **11**:2651–2661. doi: 10.1158/1078-0432.CCR-04-1564

651 Bakay M, Wang Z, Melcon G, Schiltz L, Xuan J, Zhao P, Sartorelli V, Seo J, Pegoraro E,
652 Angelini C, Shneiderman B, Escolar D, Chen Y-W, Winokur ST, Pachman LM, Fan C,
653 Mandler R, Nevo Y, Gordon E, Zhu Y, Dong Y, Wang Y, Hoffman EP. 2006. Nuclear
654 envelope dystrophies show a transcriptional fingerprint suggesting disruption of Rb-MyoD
655 pathways in muscle regeneration. *Brain* **129**:996–1013. doi:10.1093/brain/awl023

656 Bosco J, Zhou Z, Gabriëls S, Verma M, Liu N, Miller BK, Gu S, Lundberg DM, Huang Y,
657 Brown E, Josiah S, Meiyappan M, Traylor MJ, Chen N, Asakura A, De Jonge N, Blanchetot
658 C, de Haard H, Duffy HS, Keefe D. 2021. VEGFR-1/Flt-1 inhibition increases
659 angiogenesis and improves muscle function in a mouse model of Duchenne muscular

660 dystrophy. Mol Ther Methods Clin Dev. **23**:21:369-381. doi: 10.1016/j.omtm.2021.03.013
661 Bouchentouf M, Benabdallah BF, Bigey P, Yau TM, Scherman D, Tremblay JP. 2008. Vascular
662 endothelial growth factor reduced hypoxia-induced death of human myoblasts and
663 improved their engraftment in mouse muscles. *Gene Ther* **15**:404–414.
664 doi: 10.1038/sj.gt.3303059
665 Bryan BA, Walshe TE, Mitchell DC, Havumaki JS, Saint-Geniez M, Maharaj AS, Maldonado
666 AE, D'Amore PA, Bryan BA, Walshe TE, Mitchell DC, Havumaki JS, Saint-Geniez M,
667 Maharaj AS, Maldonado AE, D'Amore PA. 2008. Coordinated vascular endothelial growth
668 factor expression and signaling during skeletal myogenic differentiation. *Mol Biol Cell*
669 **19**:994–1006. doi:10.1091/mbc.E07-09-0856
670 Charville GW, Cheung TH, Yoo B, Santos PJ, Lee GK, Shrager JB, Rando TA. 2015. Ex Vivo
671 Expansion and In Vivo Self-Renewal of Human Muscle Stem Cells. *Stem cell Reports*
672 **5**:621–32. doi:10.1016/j.stemcr.2015.08.004
673 Chen YW, Zhao P, Borup R, Hoffman EP. 2000. Expression profiling in the muscular
674 dystrophies: identification of novel aspects of molecular pathophysiology. *J Cell Biol*
675 **151**:1321–36. doi:10.1083/jcb.151.6.1321
676 Chestnut B, Casie Chetty S, Koenig AL, Sumanas S. 2020. Single-cell transcriptomic analysis
677 identifies the conversion of zebrafish Etv2-deficient vascular progenitors into skeletal
678 muscle. *Nat Commun* **11**:2796. doi:10.1038/s41467-020-16515-y
679 Christov C, Chretien F, Abou-Khalil R, Bassez G, Vallet G, Authier FJ, Bassaglia Y, Shinin V,
680 Tajbakhsh S, Chazaud B, Gherardi RK. 2007. Muscle satellite cells and endothelial cells:
681 close neighbors and privileged partners. *Mol Biol Cell* **18**:1397–1409.
682 doi: 10.1091/mbc.e06-08-0693

683 De Angelis L, Berghella L, Coletta M, Lattanzi L, Zanchi M, Cusella-De Angelis MG, Ponzetto
684 C, Cossu G. 1999. Skeletal myogenic progenitors originating from embryonic dorsal aorta
685 coexpress endothelial and myogenic markers and contribute to postnatal muscle growth and
686 regeneration. *J Cell Biol* **147**:869–877. doi:10.1083/jcb.147.4.869
687 De Micheli AJ, Laurilliard EJ, Heinke CL, Ravichandran H, Fraczek P, Soueid-Baumgarten S,
688 De Vlaminck I, Elemento O, Cosgrove BD. 2020. Single-Cell Analysis of the Muscle Stem
689 Cell Hierarchy Identifies Heterotypic Communication Signals Involved in Skeletal Muscle
690 Regeneration. *Cell Rep* **30**:3583-3595.e5. doi:10.1016/j.celrep.2020.02.067
691 Delavar H, Nogueira L, Wagner PD, Hogan MC, Metzger D, Breen EC. 2014. Skeletal myofiber
692 VEGF is essential for the exercise training response in adult mice. *AJP Regul Integr Comp*
693 *Physiol* **306**:R586–R595. doi:10.1152/ajpregu.00522.2013
694 Desrochers LM, Antonyak MA, Cerione RA. 2016. Extracellular Vesicles: Satellites of
695 Information Transfer in Cancer and Stem Cell Biology. Dev Cell. 37(4):301-309. doi:
696 10.1016/j.devcel.2016.04.019.
697 Domigan CK, Warren CM, Antanesian V, Happel K, Ziyad S, Lee S, Krall A, Duan L, Torres-
698 Collado AX, Castellani LW, Elashoff D, Christofk HR, van der Bliek AM, Potente M,
699 Iruela-Arispe ML. 2015. Autocrine VEGF maintains endothelial survival through regulation
700 of metabolism and autophagy. *J Cell Sci* **128**:2236–48. doi:10.1242/jcs.163774
701 Drummond CJ, Hatley ME. 2018. A Case of mistaken identity: Rhabdomyosarcoma
702 development from endothelial progenitor cells. *Mol Cell Oncol* **5**:e1448246.
703 doi:10.1080/23723556.2018.1448246
704 Eichmann A, Marcelle C, Bréant C, Le Douarin NM. 1993. Two molecules related to the VEGF
705 receptor are expressed in early endothelial cells during avian embryonic development. *Mech*

706 *Dev* **42**:33–48. doi:10.1016/0925-4773(93)90096-g

707 Ema M, Takahashi S, Rossant J. 2006. Deletion of the selection cassette, but not cis-acting
708 elements, in targeted Flk1-lacZ allele reveals Flk1 expression in multipotent mesodermal
709 progenitors. *Blood* **107**:111–7. doi:10.1182/blood-2005-05-1970

710 Esner M, Meilhac SM, Relaix F, Nicolas J-F, Cossu G, Buckingham ME. 2006. Smooth muscle
711 of the dorsal aorta shares a common clonal origin with skeletal muscle of the myotome.
712 *Development* **133**:737–49. doi:10.1242/dev.02226

713 Fukada S, Uezumi A, Ikemoto M, Masuda S, Segawa M, Tanimura N, Yamamoto H, Miyagoe-
714 Suzuki Y, Takeda S. 2007. Molecular signature of quiescent satellite cells in adult skeletal
715 muscle. *Stem Cells* **25**:2448–59. doi:10.1634/stemcells.2007-0019

716 Gay L, Miller MR, Ventura PB, Devasthali V, Vue Z, Thompson HL, Temple S, Zong H, Cleary
717 MD, Stankunas K, Doe CQ. 2013. Mouse TU tagging: a chemical/genetic intersectional
718 method for purifying cell type-specific nascent RNA. *Genes Dev* **27**:98–115.
719 doi:10.1101/gad.205278.112

720 Gerber HP, McMurtrey A, Kowalski J, Yan M, Keyt B a, Dixit V, Ferrara N. 1998. Vascular
721 endothelial growth factor regulates endothelial cell survival through the
722 phosphatidylinositol 3'-kinase/Akt signal transduction pathway. Requirement for Flk-
723 1/KDR activation. *J Biol Chem* **273**:30336–43. doi : 10.1074/jbc.273.46.30336

724 Germani A, Di Carlo A, Mangoni A, Straino S, Giacinti C, Turrini P, Biglioli P, Capogrossi MC.
725 2003. Vascular endothelial growth factor modulates skeletal myoblast function. *Am J*
726 *Pathol* **163**:1417–1428. doi: 10.1016/S0002-9440(10)63499-2

727 Giordani L, He GJ, Negroni E, Sakai H, Law JYC, Siu MM, Wan R, Corneau A, Tajbakhsh S,
728 Cheung TH, Le Grand F. 2018. High-Dimensional Single-Cell Cartography Reveals Novel

729 Skeletal Muscle Resident Cell Populations. *SSRN Electron J* 1–13.
730 doi:10.2139/ssrn.3249467
731 Goel AJ, Rieder MK, Arnold HH, Radice GL, Krauss RS. 2017. Niche Cadherins Control the
732 Quiescence-to-Activation Transition in Muscle Stem Cells. *Cell Rep* **21**:2236–2250.
733 doi:10.1016/j.celrep.2017.10.102
734 Hardy D, Besnard A, Latil M, Jouvion G, Briand D, Thépenier C, Pascal Q, Guguin A, Gayraud-
735 Morel B, Cavaillon J-M, Tajbakhsh S, Rocheteau P, Chrétien F. 2016. Comparative Study
736 of Injury Models for Studying Muscle Regeneration in Mice. *PLoS One* **11**:e0147198.
737 doi:10.1371/journal.pone.0147198
738 Hirai H, Verma M, Watanabe S, Tastad C, Asakura Y, Asakura A. 2010. MyoD regulates
739 apoptosis of myoblasts through microRNA-mediated down-regulation of Pax3. *J Cell Biol*
740 **191**:347–65. doi:10.1083/jcb.201006025
741 Ho VC, Duan L-J, Cronin C, Liang BT, Fong G-H. 2012. Elevated vascular endothelial growth
742 factor receptor-2 abundance contributes to increased angiogenesis in vascular endothelial
743 growth factor receptor-1-deficient mice. *Circulation* **126**:741–52.
744 doi:10.1161/CIRCULATIONAHA.112.091603
745 Huang P, Schulz TJ, Beauvais A, Tseng YH, Gussoni E. 2014.
746 Intramuscular adipogenesis is inhibited by myo-endothelial progenitors with functioning
747 Bmpr1a signalling. Nat Commun. 5:4063. doi: 10.1038/ncomms5063.
748 Hutcheson DA, Kardon G. 2009. Genetic manipulations reveal dynamic cell and gene functions:
749 Cre-ating a new view of myogenesis. *Cell Cycle* **8**:3675–8. doi:10.4161/cc.8.22.9992
750 Kann AP, Krauss RS. 2019. Multiplexed RNAscope and immunofluorescence on whole-mount
751 skeletal myofibers and their associated stem cells. *Dev* **146**. doi:10.1242/dev.179259

752 Kardon G, Campbell JK, Tabin CJ. 2002. Local extrinsic signals determine muscle and
753 endothelial cell fate and patterning in the vertebrate limb. *Dev Cell* **3**:533–45.
754 doi:10.1016/s1534-5807(02)00291-5
755 Keifer OP, O'Connor DM, Boulis NM. 2014. Gene and protein therapies utilizing VEGF for
756 ALS. *Pharmacol Ther* **141**:261–71. doi:10.1016/j.pharmthera.2013.10.009
757 Kobayashi H, Butler JM, O'Donnell R, Kobayashi M, Ding B-S, Bonner B, Chiu VK, Nolan DJ,
758 Shido K, Benjamin L, Rafii S. 2010. Angiocrine factors from Akt-activated endothelial cells
759 balance self-renewal and differentiation of haematopoietic stem cells. *Nat Cell Biol*
760 **12**:1046–56. doi:10.1038/ncb2108
761 Kodippili K, Thorne PK, Laughlin MH, Duan D. 2021. Dystrophin deficiency impairs vascular
762 structure and function in the canine model of Duchenne muscular dystrophy. *J Pathol*.
763 doi:10.1002/path.5704
764 Lagha M, Brunelli S, Messina G, Cumano A, Kume T, Relaix F, Buckingham ME. 2009.
765 Pax3:Foxc2 reciprocal repression in the somite modulates muscular versus vascular cell fate
766 choice in multipotent progenitors. *Dev Cell* **17**:892–9. doi:10.1016/j.devcel.2009.10.021
767 Latroche C, Matot B, Martins-Bach A, Briand D, Chazaud B, Wary C, Carlier PG, Chrétien F,
768 Jouvion G. 2015. Structural and Functional Alterations of Skeletal Muscle Microvasculature
769 in Dystrophin-Deficient mdx Mice. *Am J Pathol* 1–13. doi:10.1016/j.ajpath.2015.05.009
770 Latroche C, Weiss-Gayet M, Muller L, Gitiaux C, Leblanc P, Liot S, Ben-Larbi S, Abou-Khalil
771 R, Verger N, Bardot P, Magnan M, Chrétien F, Mounier R, Germain S, Chazaud B. 2017.
772 Coupling between Myogenesis and Angiogenesis during Skeletal Muscle Regeneration Is
773 Stimulated by Restorative Macrophages. *Stem Cell Reports* **9**.
774 doi:10.1016/j.stemcr.2017.10.027

775 Le Grand F, Auda-Boucher G, Levitsky D, Rouaud T, Fontaine-Pérus J, Gardahaut M-F. 2004.
776 Endothelial cells within embryonic skeletal muscles: a potential source of myogenic
777 progenitors. *Exp Cell Res* **301**:232–41. doi:10.1016/j.yexcr.2004.07.028
778 Lee S, Chen TT, Barber CL, Jordan MC, Murdock J, Desai S, Ferrara N, Nagy A, Roos KP,
779 Iruela-Arispe ML. 2007. Autocrine VEGF signaling is required for vascular homeostasis.
780 *Cell* **130**:691–703. doi:10.1016/j.cell.2007.06.054
781 Li Y, Zhang F, Nagai N, Tang Z, Zhang S, Scotney P, Lennartsson J, Zhu C, Qu Y, Fang C, Hua
782 J, Matsuo O, Fong GH, Ding H, Cao Y, Becker KG, Nash A, Heldin CH, Li X. 2008.
783 VEGF-B inhibits apoptosis via VEGFR-1-mediated suppression of the expression of BH3-
784 only protein genes in mice and rats. *J Clin Invest* **118**:913–923. doi:10.1172/JCI33673
785 Linderman GC, Zhao J, Kluger Y. 2018. Zero-preserving imputation of scRNA-seq data using
786 low-rank approximation. *bioRxiv* 397588. doi**:** https://doi.org/10.1101/397588
787 Liu L, Cheung TH, Charville GW, Rando T a. 2015. Isolation of skeletal muscle stem cells by
788 fluorescence-activated cell sorting. *Nat Protoc* **10**:1612–1624. doi:10.1038/nprot.2015.110
789 Liu Y, Berendsen AD, Jia S, Lotinun S, Baron R, Ferrara N, Olsen BR. 2012. Intracellular
790 VEGF regulates the balance between osteoblast and adipocyte differentiation. *J Clin Invest*
791 **122**:3101–3113. doi:10.1172/JCI61209
792 Loiben AM, Soueid-Baumgarten S, Kopyto RF, Bhattacharya D, Kim JC, Cosgrove BD. 2017.
793 Data-Modeling Identifies Conflicting Signaling Axes Governing Myoblast Proliferation and
794 Differentiation Responses to Diverse Ligand Stimuli. *Cell Mol Bioeng* **10**:433–450.
795 doi:10.1007/s12195-017-0508-5
796 Mac Gabhann F, Qutub AA, Annex BH, Popel AS. 2011. Systems biology of pro-angiogenic
797 therapies targeting the VEGF system. *Wiley Interdiscip Rev Syst Biol Med* **2**:694–707.

798 doi:10.1002/wsbm.92

799 Mayeuf-Louchart A, Lagha M, Danckaert A, Rocancourt D, Relaix F, Vincent SD, Buckingham
800 M. 2014. Notch regulation of myogenic versus endothelial fates of cells that migrate from
801 the somite to the limb. *Proc Natl Acad Sci U S A* **111**:8844–8849.
802 doi:10.1073/pnas.1407606111

803 Mayeuf-Louchart A, Montarras D, Bodin C, Kume T, Vincent SD, Buckingham M. 2016.
804 Endothelial cell specification in the somite is compromised in Pax3-positive progenitors of
805 Foxc1/2 conditional mutants, with loss of forelimb myogenesis. *Development* **143**:872–9.
806 doi:10.1242/dev.128017

807 Mercatelli N, Dimauro I, Ciafré SA, Farace MG, Caporossi D. 2010. AlphaB-crystallin is
808 involved in oxidative stress protection determined by VEGF in skeletal myoblasts. *Free*
809 *Radic Biol Med* **49**:374–82. doi:10.1016/j.freeradbiomed.2010.04.027

810 Messina S, Mazzeo A, Bitto A, Aguennouz M, Migliorato A, De Pasquale MG, Minutoli L,
811 Altavilla D, Zentilin L, Giacca M, Squadrito F, Vita G. 2007. VEGF overexpression via
812 adeno-associated virus gene transfer promotes skeletal muscle regeneration and enhances
813 muscle function in mdx mice. *FASEB J* **21**:3737–3746. doi : 10.1096/fj.07-8459com

814 Minasi MG, Riminucci M, De Angelis L, Borello U, Berarducci B, Innocenzi A, Caprioli A,
815 Sirabella D, Baiocchi M, De Maria R, Boratto R, Jaffredo T, Broccoli V, Bianco P, Cossu G.
816 2002. The meso-angioblast: a multipotent, self-renewing cell that originates from the dorsal
817 aorta and differentiates into most mesodermal tissues. *Development* **129**:2773–83. doi:
818 10.1242/dev.129.11.2773

819 Miquerol L, Gertsenstein M, Harpal K, Rossant J, Nagy a. 1999. Multiple developmental roles
820 of VEGF suggested by a LacZ-tagged allele. *Dev Biol* **212**:307–322.

821 doi:10.1006/dbio.1999.9355

822 Motohashi N, Asakura A. 2014. Muscle satellite cell heterogeneity and self-renewal. *Front Cell*
823 *Dev Biol* **2**:1–11. doi:10.3389/fcell.2014.00001

824 Motohashi N, Asakura Y, Asakura A. 2014. Isolation, culture, and transplantation of muscle
825 satellite cells. *J Vis Exp* 1–7. doi:10.3791/50846

826 Motoike T, Markham DW, Rossant J, Sato TN. 2003. Evidence for novel fate of Flk1+
827 progenitor: contribution to muscle lineage. *Genesis* **35**:153–9. doi:10.1002/gene.10175

828 Murach KA, Vechetti IJ, Van Pelt DW, Crow SE, Dungan CM, Figueiredo VC, Kosmac K, Fu X,
829 Richards CI, Fry CS, McCarthy JJ, Peterson CA. 2020. Fusion-Independent Satellite Cell
830 Communication to Muscle Fibers During Load-Induced Hypertrophy. *Function* **1**:1–15.
831 doi:10.1093/function/zqaa009

832 Murphy MM, Lawson J a, Mathew SJ, Hutcheson D a, Kardon G. 2011. Satellite cells,
833 connective tissue fibroblasts and their interactions are crucial for muscle regeneration. *J*
834 *Cell Sci* **124**:e1–e1. doi:10.1242/jcs098228

835 Noren DP, Chou WH, Lee SH, Qutub AA, Warmflash A, Wagner DS, Popel AS, Levchenko A.
836 2016. Endothelial cells decode VEGF-mediated Ca2+ signaling patterns to produce distinct
837 functional responses. *Sci Signal* **9**:ra20–ra20. doi:10.1126/scisignal.aad3188

838 Okabe K, Kobayashi S, Yamada T, Kurihara T, Tai-nagara I. 2014. Neurons Limit Angiogenesis
839 by Titrating VEGF in Retina. *Cell* **159**:584–596. doi:10.1016/j.cell.2014.09.025

840 Olfert IM, Howlett RA, Tang K, Dalton ND, Gu Y, Peterson KL, Wagner PD, Breen EC. 2009.
841 Muscle-specific VEGF deficiency greatly reduces exercise endurance in mice. *J Physiol*
842 **587**:1755–1767. doi: : 10.1113/jphysiol.2008.164384

843 Pallafacchina G, François S, Regnault B, Czarny B, Dive V, Cumano A, Montarras D,

844 Buckingham M. 2010. An adult tissue-specific stem cell in its niche: a gene profiling
845 analysis of in vivo quiescent and activated muscle satellite cells. *Stem Cell Res* **4**:77–91.
846 doi:10.1016/j.scr.2009.10.003
847 Pertea M, Kim D, Pertea GM, Leek JT, Salzberg SL. 2016. Transcript-level expression analysis
848 of RNA-seq experiments with HISAT, StringTie and Ballgown. *Nat Protoc* **11**:1650–1667.
849 doi:10.1038/nprot.2016.095
850 Podkalicka P, Mucha O, Kaziród K, Bronisz-Budzyńska I, Ostrowska-Paton S, Tomczyk M,
851 Andrysiak K, Stępniewski J, Dulak J, Łoboda A. 2021. Age-Dependent Dysregulation of
852 Muscle Vasculature and Blood Flow Recovery after Hindlimb Ischemia in the mdx Model
853 of Duchenne Muscular Dystrophy. Biomedicines. 9:481. doi:
854 10.3390/biomedicines9050481.
855 Poesen K, Lambrechts D, Van Damme P, Dhondt J, Bender F, Frank N, Bogaert E, Claes B,
856 Heylen L, Verheyen A, Raes K, Tjwa M, Eriksson U, Shibuya M, Nuydens R, Van Den
857 Bosch L, Meert T, D'Hooge R, Sendtner M, Robberecht W, Carmeliet P. 2008. Novel Role
858 for Vascular Endothelial Growth Factor (VEGF) Receptor-1 and Its Ligand VEGF-B in
859 Motor Neuron Degeneration. *J Neurosci* **28**:10451–10459. doi:10.1523/JNEUROSCI.1092-
860 08.2008
861 Roobrouck VD, Clavel C, Jacobs SA, Ulloa-Montoya F, Crippa S, Sohni A, Roberts SJ, Luyten
862 FP, Van Gool SW, Sampaolesi M, Delforge M, Luttun A, Verfaillie CM. 2011.
863 Differentiation potential of human postnatal mesenchymal stem cells, mesoangioblasts, and
864 multipotent adult progenitor cells reflected in their transcriptome and partially influenced by
865 the culture conditions. *Stem Cells* **29**:871–82. doi:10.1002/stem.633
866 RStudio Team. 2020. RStudio: Integrated Development for R. RStudio, PBC, Boston, MA.

867 http://www.rstudio.com/

868 Ryall JG, Dell'Orso S, Derfoul A, Juan A, Zare H, Feng X, Clermont D, Koulnis M, Gutierrez-
869 Cruz G, Fulco M, Sartorelli V. 2015. The NAD+-dependent sirt1 deacetylase translates a
870 metabolic switch into regulatory epigenetics in skeletal muscle stem cells. *Cell Stem Cell*
871 **16**:171–183. doi:10.1016/j.stem.2014.12.004

872 Sakurai H, Okawa Y, Inami Y, Nishio N, Isobe K. 2008. Paraxial mesodermal progenitors
873 derived from mouse embryonic stem cells contribute to muscle regeneration via
874 differentiation into muscle satellite cells. *Stem Cells* **26**:1865–73.
875 doi:10.1634/stemcells.2008-0173

876 Schindelin J, Arganda-Carreras I, Frise E, Kaynig V, Longair M, Pietzsch T, Preibisch S,
877 Rueden C, Saalfeld S, Schmid B, Tinevez J-Y, White DJ, Hartenstein V, Eliceiri K,
878 Tomancak P, Cardona A. 2012. Fiji: an open-source platform for biological-image analysis.
879 *Nat Methods* **9**:676–82. doi:10.1038/nmeth.2019

880 Stuart T, Butler A, Hoffman P, Hafemeister C, Papalexi E, Mauck WM, Hao Y, Stoeckius M,
881 Smibert P, Satija R. 2019. Comprehensive Integration of Single-Cell Data. *Cell* **177**:1888-
882 1902.e21. doi:10.1016/j.cell.2019.05.031

883 Tamaki T, Akatsuka A, Ando K, Nakamura Y, Matsuzawa H, Hotta T, Roy RR, Edgerton VR.
884 2002. Identification of myogenic-endothelial progenitor cells in the interstitial spaces of
885 skeletal muscle. *J Cell Biol* **157**:571–7. doi:10.1083/jcb.200112106

886 Tang K, Breen EC, Gerber H-P, Ferrara NM a, Wagner PD. 2004. Capillary regression in
887 vascular endothelial growth factor-deficient skeletal muscle. *Physiol Genomics* **18**:63–69.
888 doi:10.1152/physiolgenomics.00023.2004

889 Torre E, Dueck H, Shaffer S, Gospocic J, Gupte R, Bonasio R, Kim J, Murray J, Raj A. 2018.

890 Rare Cell Detection by Single-Cell RNA Sequencing as Guided by Single-Molecule RNA
891 FISH. *Cell Syst* **6**:171-179.e5. doi:10.1016/j.cels.2018.01.014
892 Tozer S, Bonnin M-A, Relaix F, Di Savino S, García-Villalba P, Coumailleau P, Duprez D. 2007.
893 Involvement of vessels and PDGFB in muscle splitting during chick limb development.
894 *Development* **134**:2579–91. doi:10.1242/dev.02867
895 Tseng BS, Zhao P, Pattison JS, Gordon SE, Granchelli JA, Madsen RW, Folk LC, Hoffman EP,
896 Booth FW. 2002. Regenerated mdx mouse skeletal muscle shows differential mRNA
897 expression. *J Appl Physiol* **93**:537–45. doi:10.1152/japplphysiol.00202.2002
898 Turaç G, Hindley CJ, Thomas R, Davis JA, Deleidi M, Karaöz E, Pruszak J. 2013. Combined
899 Flow Cytometric Analysis of Surface and Intracellular Antigens Reveals Surface Molecule
900 Markers of Human Neuropoiesis. *PLoS One* **8**:1–14. doi:10.1371/journal.pone.0068519
901 van Velthoven CTJ, de Morree A, Egner IM, Brett JO, Rando TA. 2017. Transcriptional
902 Profiling of Quiescent Muscle Stem Cells In Vivo. *Cell Rep* **21**:1994–2004.
903 doi:10.1016/j.celrep.2017.10.037
904 Veldman MB, Zhao C, Gomez G a, Lindgren AG, Huang H, Yang H, Yao S, Martin BL,
905 Kimelman D, Lin S. 2013. Transdifferentiation of fast skeletal muscle into functional
906 endothelium in vivo by transcription factor etv2. *PLoS Biol* **11**:e1001590.
907 doi:10.1371/journal.pbio.1001590
908 Vempati P, Popel AS, Mac Gabhann F. 2014. Extracellular regulation of VEGF: Isoforms,
909 proteolysis, and vascular patterning. *Cytokine Growth Factor Rev* **25**:1–19.
910 doi:10.1016/j.cytogfr.2013.11.002
911 Verma M, Asakura Y, Hirai H, Watanabe S, Tastad C, Fong G-H, Ema M, Call JA, Lowe DA,
912 Asakura A. 2010. Flt-1 haploinsufficiency ameliorates muscular dystrophy phenotype by

913 developmentally increased vasculature in mdx mice. *Hum Mol Genet* **19**:4145–59.
914 doi:10.1093/hmg/ddq334
915 Verma M, Asakura Y, Murakonda BSR, Pengo T, Latroche C, Chazaud B, McLoon LK,
916 Asakura A. 2018. Muscle Satellite Cell Cross-Talk with a Vascular Niche Maintains
917 Quiescence via VEGF and Notch Signaling. *Cell Stem Cell* **23**:530-543.e9.
918 doi:10.1016/j.stem.2018.09.007
919 Verma M, Shimizu-Motohashi Y, Asakura Y, Ennen JP, Bosco J, Zhou Z, Fong G, Josiah S,
920 Keefe D, Asakura A. 2019. Inhibition of FLT1 ameliorates muscular dystrophy phenotype
921 by increased vasculature in a mouse model of Duchenne muscular dystrophy. *PLOS Genet*
922 **15**:e1008468. doi:10.1371/journal.pgen.1008468
923 Vieira NM, Elvers I, Alexander MS, Moreira YB, Eran A, Gomes JP, Marshall JL, Karlsson EK,
924 Verjovski-Almeida S, Lindblad-Toh K, Kunkel LM, Zatz M. 2015. Jagged 1 Rescues the
925 Duchenne Muscular Dystrophy Phenotype. *Cell* **163**:1204–1213.
926 doi:10.1016/j.cell.2015.10.049
927 Wagner PD, Olfert IM, Tang K, Breen EC. 2006. Muscle-targeted deletion of VEGF and
928 exercise capacity in mice. *Respir Physiol Neurobiol* **151**:159–166.
929 doi:10.1016/j.resp.2005.09.007
930 Xin C, Chu X, Wei W, Kuang B, Wang Y, Tang Y, Chen J, You H, Li C, Wang B. 2021.
931 Combined gene therapy via VEGF and mini-dystrophin synergistically improves
932 pathologies in temporalis muscle of dystrophin/utrophin double knockout mice. Hum Mol
933 Genet. 30:1349-1359. doi: 10.1093/hmg/ddab120.
934 Yan G, Yan R, Chen C, Chen C, Zhao Y, Qin W, Veldman MB, Li S, Lin S. 2019. Engineering
935 vascularized skeletal muscle tissue with transcriptional factor ETV2-induced autologous

936 endothelial cells. *Protein Cell* **10**:217–222. doi:10.1007/s13238-018-0542-7

937 Yan H, Guo Y, Zhang P, Zu L, Dong X, Chen L, Tian J, Fan X, Wang N, Wu X, Gao W. 2005.
938 Superior neovascularization and muscle regeneration in ischemic skeletal muscles following
939 VEGF gene transfer by rAAV1 pseudotyped vectors. *Biochem Biophys Res Commun*
940 **336**:287–298. doi: 10.1016/j.bbrc.2005.08.066

941 Young MD, Behjati S. 2020. SoupX removes ambient RNA contamination from droplet based
942 single-cell RNA sequencing data. *bioRxiv* 303727. doi:10.1101/303727

943 Yue L, Wan R, Luan S, Zeng W, Cheung TH. 2020. Dek Modulates Global Intron Retention
944 during Muscle Stem Cells Quiescence Exit. *Dev Cell* **53**:661-676.e6.
945 doi:10.1016/j.devcel.2020.05.006

946 Zhang MJ, Ntranos V, Tse D. 2020. Determining sequencing depth in a single-cell RNA-seq
947 experiment. *Nat Commun* **11**:1–11. doi:10.1038/s41467-020-14482-y

948

949

950 **Figure Legends**

951

952 **Figure 1. EC gene signal including VEGF receptor genes in MuSCs.**

953 A) Experimental schema for bulk and single cell sequencing from the
954 *Pax7*^{CreERT2}*:R26R*^{tdT}*:Flk1*^{GFP} mice. Bulk sequencing performed on MuSCs, ECs and
955 single muscle fibers (SMFs) from uninjured muscle. FACS sorted MuSCs and ECs from
956 uninjured and regenerating TA muscle (3 days following CTX) were run separately on
957 the 10X single cell platform and aggregated.

958 B) Bulk RNAseq showing EC signature in MuSCs. Subset dividing genes that are
959 commonly used to delineate cell identity for MuSCs, ECs and SMFs. Last column shows
960 genes that define macrophages (Mφ), which should not be highly expressed in any on our
961 cell types. Red dots indicate MuSCs, green dots indicate ECs and blue dots indicate
962 SMFs.

963 C) UMAP from aggregated single cell RNAseq shows expression of different phases of
964 MuSCs (quiescent MuSCs, activated MuSCs and myoblasts), ECs (tip ECs and ECs) and
965 from likely contaminant cells such as macrophages (Mφ) and smooth muscle cells
966 (SMC).

967 D) UMAP from aggregated data visualized by sample day showing MuSCs segregated by
968 the sample day but overlap in the EC population. Red dots indicate intact (day 0) and
969 blue dots indicate 3 days following CTX.

970 E) Expression of quality control genes such as *eGFP*, *tdTomato*, *CreERT2* and EC genes
971 such as *Cdh5*, *Kdr* and *Flt1*.

972 F) Genome browser tracks of whole muscle and TU-tagged MuSC nascent RNA
973 (GSE97399, Velthoven et al., 2017). *Kdr* and *Pecam1* expression can be found in the
974 MuSC fraction. As control, *Myh1* is highly expressed in the whole muscle preparation but
975 largely absent in the MuSC fraction. *Sdc4* and *Calcr* are highly expressed in MuSC and
976 less so in the whole muscle fraction.
977 G) qPCR for *Kdr, Flt1, Nrp1* and *Nrp2* in EC lines (B.end3 and C166), muscle cell line
978 (C2C12) and MuSC-derived myoblasts in growth and differentiation medium (DM)
979 shows low level expression of VEGFRs and VEGF co-receptors.
980 H) RNAScope of *Flt1* on freshly isolated single muscle fibers from *Pax7*^{tdT} mice shows *Flt1*
981 expression (green) and tdTomato (red) in MuSCs. Nuclei were counterstained with DAPI
982 (blue). Scale bar indicates 5 µm.
983 I) Immunostaining for PECAM1, VE-cadherin (VE-Cad), VEGFA co-receptors (NRP1 and
984 NRP2) and VEGFA receptors (FLT1 and FLK1) in B.End3 EC cell line and MuSC-
985 derived myoblasts (MB). Nuclei were counterstained with DAPI (blue). Scale bar
986 indicates 20 µm.

987

988 **Figure 2. VEGFA-FLT1-AKT1 axis controls apoptosis in MuSC *in vitro.***
989 A) Immunostaining for VEGFA (green) in MuSC-derived myoblasts. Nuclei were
990 counterstained with DAPI (blue). Scale bar indicates 20 µm.
991 B) Experimental scheme for assessing apoptosis following thapsagargin induction in
992 myoblast culture.
993 C) Decreased cell survival in myoblast *in vitro* as VEGFA is blocked using FLT1-FC (a
994 VEFGA trap). This phenotype is partially rescued with exogenous VEGFA (50 ng/ml).

995 D) Graphical representation of the VEGF pathway inhibitors used in panel D.

996 E) Following thapsagargin induction, apoptotic and necrotic cells are increased with
997 inhibition of FLT1 via FLT1-FC or anti-FLT1 antibody (anti-FLT1 mAb) but not FLK1
998 (SU5402 and ZM306416) or NRP1-FLK1 inhibition (EG00229) following exogenous
999 VEGFA (50 ng/ml).

1000 F) 4-OHT induced deletion of *Flt1* in $Pax7^{+/CreER}$:$Flt1^{Loxp/Loxp}$ myoblasts is sufficient to
1001 reduce cell survival in myoblast without induction of apoptosis.

1002 G) Cell survival is decreased *in vitro* in myoblast with thapsagargine induction following 4-
1003 OHT mediated deletion of *Flt1* in $Pax7^{+/CreER}$:$Flt1^{Loxp/Loxp}$ myoblast that is not rescued by
1004 exogenous VEGFA. Blue indicates *MuSC-*$Flt1^{+/+}$, red indicates *MuSC-*$Flt1^{+/+}$ with 50
1005 ng/ml VEGFA, green indicates *MuSC-*$Flt1^{\Delta/\Delta}$ and purple indicates *MuSC-*$Flt1^{\Delta/\Delta}$ with 50
1006 ng/ml VEGFA.

1007 H) Representative images of pAKT (red) in myoblast stained by MyoD (green) in *MuSC-*
1008 $Flt1^{+/+}$ and *MuSC-*$Flt1^{\Delta/\Delta}$ myoblasts induced with exogenous VEGFA. Nuclei were
1009 counterstained with DAPI (blue). Scale bar indicates 50 µm.

1010 I) Quantification of pAKT in myoblasts stained by MyoD in *MuSC-*$Flt1^{+/+}$ and *MuSC-*
1011 $Flt1^{\Delta/\Delta}$ myoblast induced w/wo exogenous VEGFA. VEGFA induction increases pAKT
1012 in *MuSC-*$Flt1^{+/+}$ myoblasts but this response is lost in *MuSC-*$Flt1^{\Delta/\Delta}$ myoblasts.

1013 J) Annexin V quantification of myoblasts transfected with myr-AKT and E4ORF1 to
1014 activate AKT1 showed increased cell survival of myoblasts following apoptosis
1015 induction.

1016 K) Representative model for VEGFA-FLT1-AKT axis-mediated MuSC survival.

1017

1018 **Figure 3. MuSC-derived *VEGFA* and *Flt1* requires proper skeletal muscle.**

1019 A) Experimental schema detailing the experiments performed in this figure. The
1020 *Pax7*$^{+/CreER}$*:R26R*^{tdT}*:VEGFA*$^{+/Hyper}$ (*VEGFA*$^{+/Hyper}$) *Pax7*$^{+/CreER}$*:R26R*^{tdT}*:VEGFA*$^{Loxp/Loxp}$
1021 *for MuSC-VEGFA*$^{\Delta/\Delta}$ and *Pax7*^{tdT}*:Flt1*$^{Loxp/Loxp}$ for *MuSC-Flt1*$^{\Delta/\Delta}$ lines were pulsed with
1022 tamoxifen (TMX) prior to investigation.

1023 B) Representative H&E-stained images for intact and on 14-day post injury TA muscle from
1024 *MuSC-VEGFA*$^{+/Hyper}$*, MuSC-Flt1*$^{\Delta/\Delta}$ *and MuSC-VEGFA*$^{\Delta/\Delta}$ mice and their representative
1025 controls. Scale bar indicates 50 µm.

1026 C) Annexin V staining show less necrotic cells in MuSC from *VEGFA*$^{+/Hyper}$ mice compared
1027 with the control one day following injury.

1028 D) Quantification of MuSCs from single muscle fibers show increased MuSCs in
1029 *VEGFA*$^{+/Hyper}$ EDL muscle compared with the control mice at base line and 14 days post
1030 injury.

1031 E) Fiber size distribution and F) mean feret's diameter of uninjured and regenerating muscle
1032 14 days post injury from *VEGFA*$^{+/Hyper}$ and control mice show no difference at baseline
1033 but an increase in fiber diameter following injury.

1034 G) Annexin V staining show increased dead cells in MuSCs from *MuSC-VEGFA*$^{\Delta/\Delta}$ mice
1035 one day following CTX compared with the control *MuSC-VEGFA*$^{+/+}$ mice.

1036 H) Quantification of MuSCs from single muscle fiber at base line and 14 days post injury.

1037 I) Fiber size distribution and J) mean feret's diameter of uninjured and regenerating muscle
1038 14 days post injury from *MuSC-VEGFA*$^{\Delta/\Delta}$ and *MuSC-VEGFA*$^{+/+}$ mice show no
1039 difference at baseline but a decrease in fiber diameter following injury.

1040 K) Annexin V staining show increased apoptosis in MuSCs from *MuSC-Flt1*$^{\Delta/\Delta}$ mice one
1041 day following injury compared with the control *MuSC-Flt1*$^{+/+}$ mice.
1042 L) Quantification of MuSCs from single muscle fiber show decreased MuSCs in *MuSC-*
1043 *Flt1*$^{\Delta/\Delta}$ EDL muscle at base line and 14 days post injury compared with the control
1044 *MuSC-Flt1*$^{+/+}$ mice.
1045 M) Fiber size distribution and N) mean feret's diameter of uninjured and regenerating muscle
1046 from *MuSC-Flt1*$^{\Delta/\Delta}$ and compared with the control *MuSC-Flt1*$^{+/+}$ mice show no
1047 difference at baseline but a decrease in fiber diameter following injury.
1048

1049 **Figure 4. VEGFA-FLT1 pathway in MuSCs regulates muscle pathology in DMD model**
1050 **mice.**
1051 A) Experimental schema detailing the experiments performed in this figure. The
1052 *mdx:Pax7*^{tdT}*:Flt1*$^{Loxp/Loxp}$ was pulsed with tamoxifen (TMX) to generate *mdx:MuSC-*
1053 *Flt1*$^{\Delta/\Delta}$ mice prior to investigation. *mdx*:*VEGFA*$^{+/Hyper}$ mouse line was used without any
1054 induction.
1055 B) Representative H&E and Sirus red stain from *mdx:MuSC-Flt1*$^{+/+}$ and *mdx:MuSC-Flt1*$^{\Delta/\Delta}$
1056 mouse TA muscle at 3 months of age. Scale bar indicates 50 µm.
1057 C) Smaller average fiber size in *mdx:MuSC-Flt1*$^{\Delta/\Delta}$ compared with the control *mdx:MuSC-*
1058 *Flt1*$^{+/+}$ mouse TA muscle.
1059 D) Increased fibrotic area in *mdx:MuSC-Flt1*$^{\Delta/\Delta}$ compared with the control *mdx:MuSC-*
1060 *Flt1*$^{+/+}$ mouse TA muscle.
1061 E) Decreased muscle perfusion in *mdx:MuSC-Flt1*$^{\Delta/\Delta}$ compared with the control *mdx:MuSC-*
1062 *Flt1*$^{+/+}$ mouse TA muscle.

1063 F) Decreased grip strength normalized to body weight in *mdx:MuSC-Flt1*$^{\Delta/\Delta}$ compared with
1064 the control *mdx:MuSC-Flt1*$^{+/+}$ mouse TA muscle at both 3 and 12 months of age.
1065 G) Representative H&E and Sirus red stain from *mdx*:*VEGFA*$^{+/Hyper}$ and *mdx*:*VEGFA*$^{+/+}$
1066 mouse TA muscle at 3 months from TA muscle (top four panels) and diaphragm muscle
1067 (bottom four panels).
1068 H) Increased average fiber size in *mdx*:*VEGFA*$^{+/Hyper}$ compared with the control
1069 *mdx*:*VEGFA*$^{+/+}$ mouse TA and diaphragm (DM) muscle. Scale bar indicates 50 µm.
1070 I) Decreased fibrosis in *mdx*:*VEGFA*$^{+/Hyper}$ compared with the control *mdx*:*VEGFA*$^{+/+}$
1071 mouse TA and diaphragm (DM) muscle
1072 J) Muscle perfusion is increased in *mdx*:*VEGFA*$^{+/Hyper}$ compared with the control
1073 *mdx*:*VEGFA*$^{+/+}$ mouse TA muscle.
1074 K) Grip strength normalized to body weight is increased in *mdx*:*VEGFA*$^{+/Hyper}$ compared
1075 with the control *mdx*:*VEGFA*$^{+/+}$ mice.

Figure 1

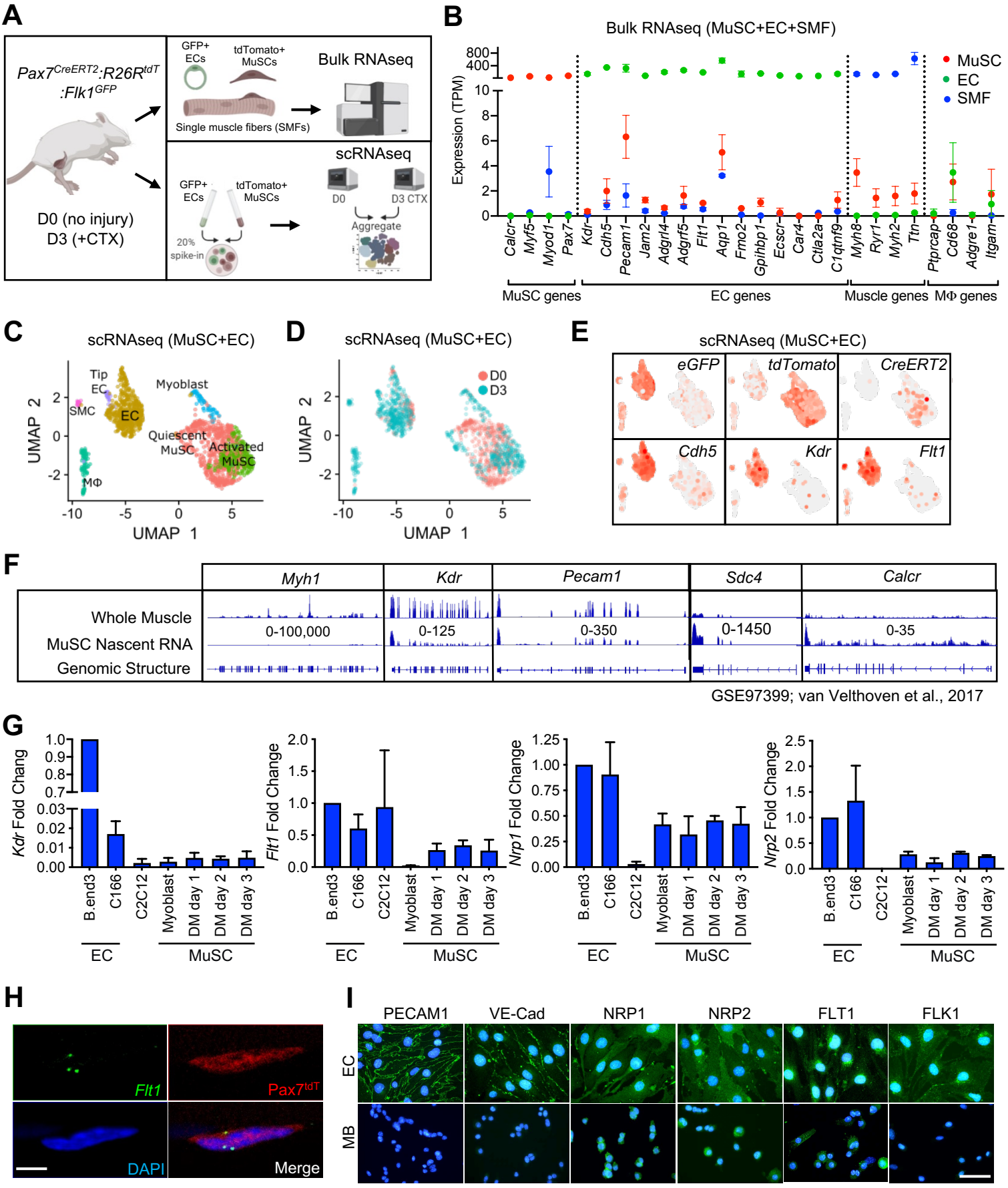
A
Pax7CreERT2:R26RtdT:Flk1GFP
D0 (no injury)
D3 (+CTX)
GFP+ ECs
tdTomato+ MuSCs
Single muscle fibers (SMFs)
Bulk RNAseq
scRNAseq
D0
D3 CTX
Aggregate
20% spike-in
B
Bulk RNAseq (MuSC+EC+SMF)
Expression (TPM)
MuSC
EC
SMF
Calcr Myf5 Myod1 Pax7 Kdr Cdh5 Pecam1 Jam2 Adgrl4 Adgrf5 Flt1 Aqp1 Fmo2 Gpihbp1 Ecscr Car4 Ctla2a C1qtnf9 Myh8 Ryr1 Myh2 Ttn Ptprcap Cd68 Adgre1 Itgam
MuSC genes
EC genes
Muscle genes
MΦ genes
C
scRNAseq (MuSC+EC)
Tip EC
SMC
EC
Myoblast
Quiescent MuSC
Activated MuSC
MΦ
UMAP 2
UMAP 1
D
scRNAseq (MuSC+EC)
D0
D3
UMAP 2
UMAP 1
E
scRNAseq (MuSC+EC)
eGFP
tdTomato
CreERT2
Cdh5
Kdr
Flt1
F
Myh1
Kdr
Pecam1
Sdc4
Calcr
Whole Muscle
MuSC Nascent RNA
Genomic Structure
0-100,000
0-125
0-350
0-1450
0-35
GSE97399; van Velthoven et al., 2017
G
Kdr Fold Chang
Flt1 Fold Change
Nrp1 Fold Change
Nrp2 Fold Change
B.end3
C166
C2C12
Myoblast
DM day 1
DM day 2
DM day 3
EC
MuSC
H
Flt1
Pax7tdT
DAPI
Merge
I
PECAM1
VE-Cad
NRP1
NRP2
FLT1
FLK1
EC
MB

Figure 2

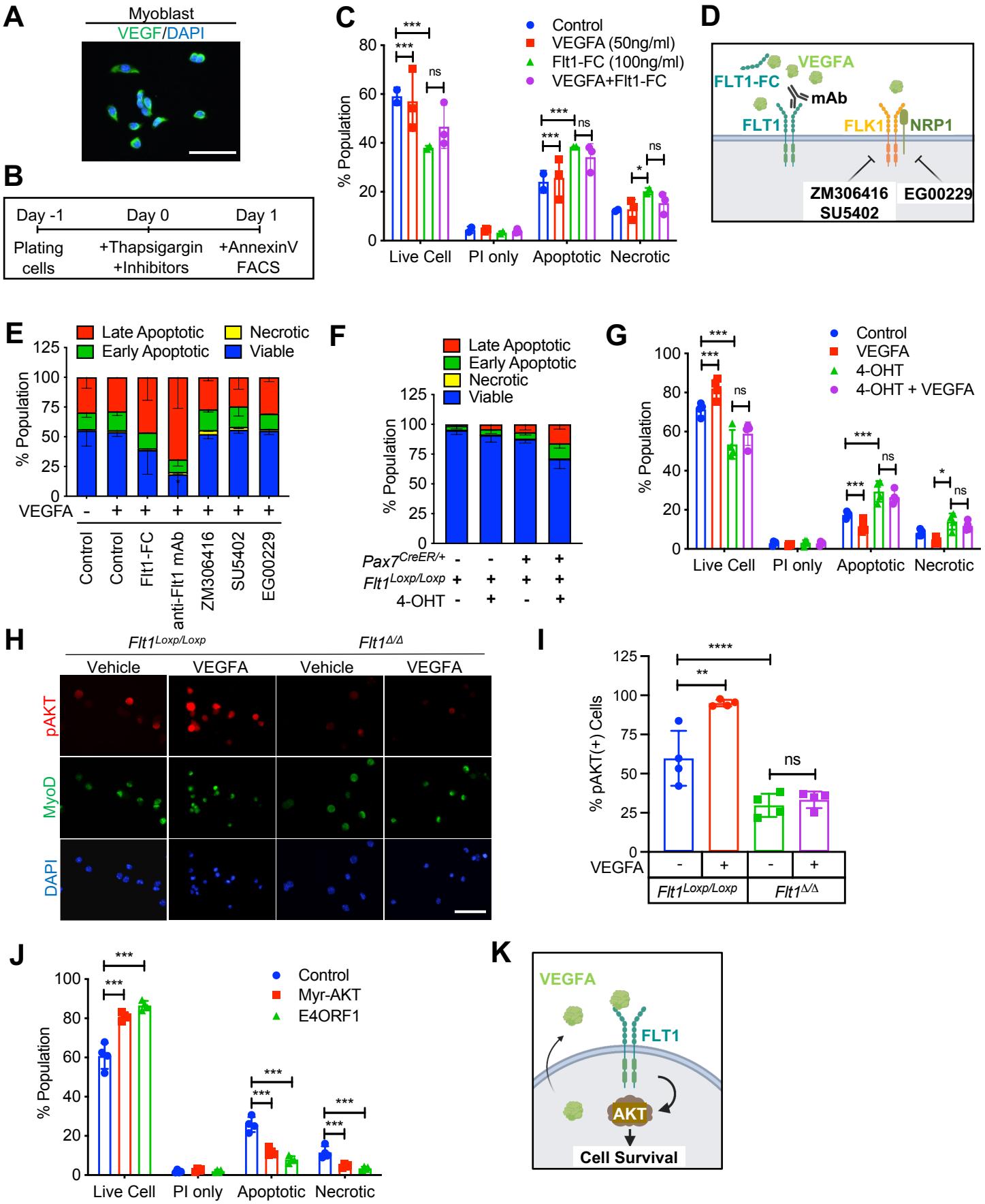
A
Myoblast
VEGF/DAPI
B
Day -1
Day 0
Day 1
Plating cells
+Thapsigargin +Inhibitors
+AnnexinV FACS
C
Control
VEGFA (50ng/ml)
Flt1-FC (100ng/ml)
VEGFA+Flt1-FC
% Population
Live Cell
PI only
Apoptotic
Necrotic
D
VEGFA
FLT1-FC
mAb
FLT1
FLK1
NRP1
ZM306416
SU5402
EG00229
E
Late Apoptotic
Early Apoptotic
Necrotic
Viable
% Population
VEGFA
Control
Control
Flt1-FC
anti-Flt1 mAb
ZM306416
SU5402
EG00229
F
Late Apoptotic
Early Apoptotic
Necrotic
Viable
% Population
Pax7CreER/+
Flt1Loxp/Loxp
4-OHT
G
Control
VEGFA
4-OHT
4-OHT + VEGFA
% Population
Live Cell
PI only
Apoptotic
Necrotic
H
Flt1Loxp/Loxp
Flt1Δ/Δ
Vehicle
VEGFA
Vehicle
VEGFA
pAKT
MyoD
DAPI
I
% pAKT(+) Cells
VEGFA
Flt1Loxp/Loxp
Flt1Δ/Δ
J
Control
Myr-AKT
E4ORF1
% Population
Live Cell
PI only
Apoptotic
Necrotic
K
VEGFA
FLT1
AKT
Cell Survival

Figure 3

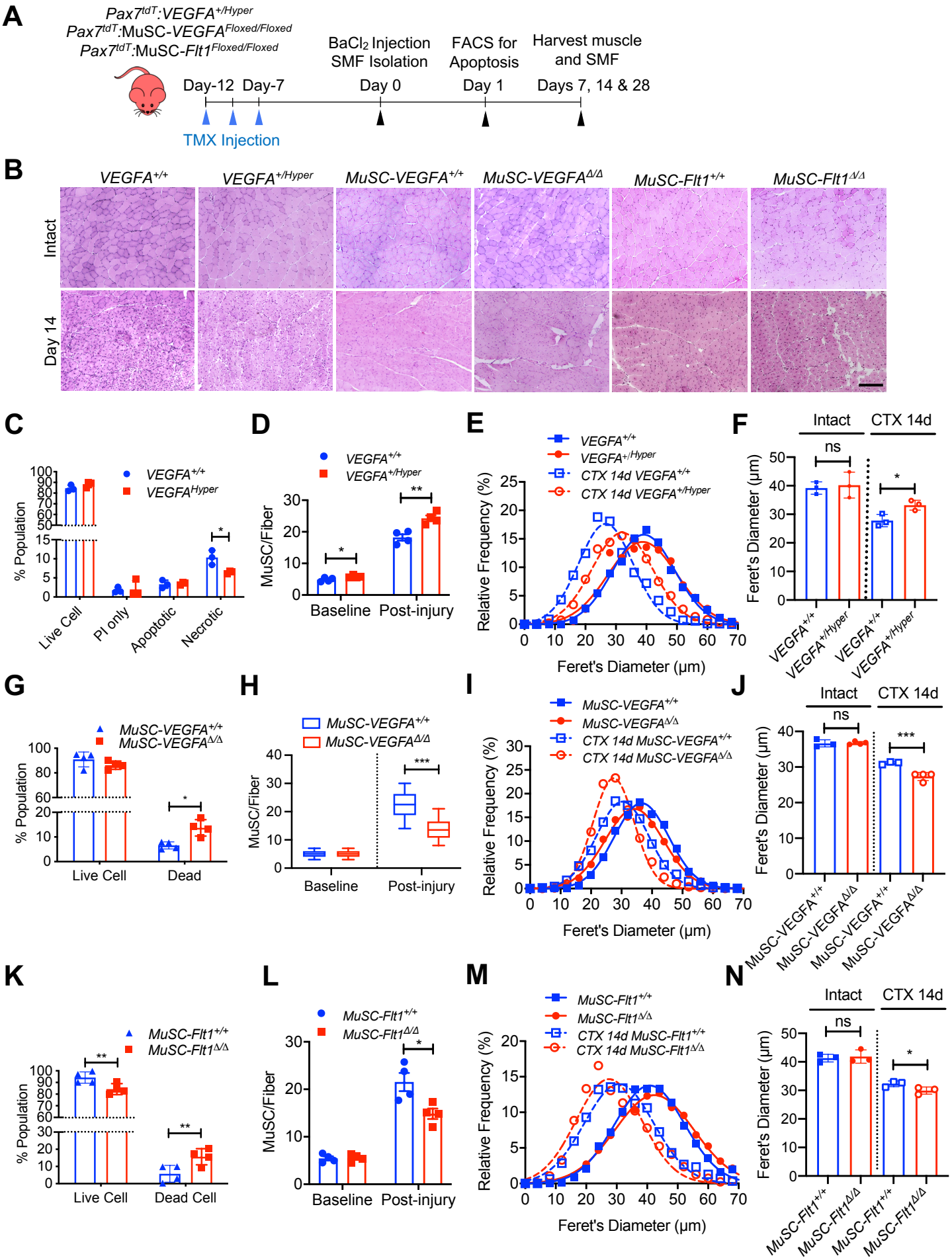
A
Pax7tdT:VEGFA+/Hyper
Pax7tdT:MuSC-VEGFAFloxed/Floxed
Pax7tdT:MuSC-Flt1Floxed/Floxed
BaCl2 Injection
SMF Isolation
FACS for Apoptosis
Harvest muscle and SMF
Day-12 Day-7
Day 0
Day 1
Days 7, 14 & 28
TMX Injection
B
VEGFA+/+
VEGFA+/Hyper
MuSC-VEGFA+/+
MuSC-VEGFAΔ/Δ
MuSC-Flt1+/+
MuSC-Flt1Δ/Δ
Intact
Day 14
C
% Population
VEGFA+/+
VEGFAHyper
Live Cell
PI only
Apoptotic
Necrotic
D
MuSC/Fiber
Baseline
Post-injury
E
Relative Frequency (%)
CTX 14d VEGFA+/+
CTX 14d VEGFA+/Hyper
Feret's Diameter (µm)
F
Intact
CTX 14d
ns
Feret's Diameter (µm)
G
MuSC-VEGFA+/+
MuSC-VEGFAΔ/Δ
Live Cell
Dead
H
I
CTX 14d MuSC-VEGFA+/+
CTX 14d MuSC-VEGFAΔ/Δ
J
K
MuSC-Flt1+/+
MuSC-Flt1Δ/Δ
Dead Cell
L
M
CTX 14d MuSC-Flt1+/+
CTX 14d MuSC-Flt1Δ/Δ
N

Figure 4

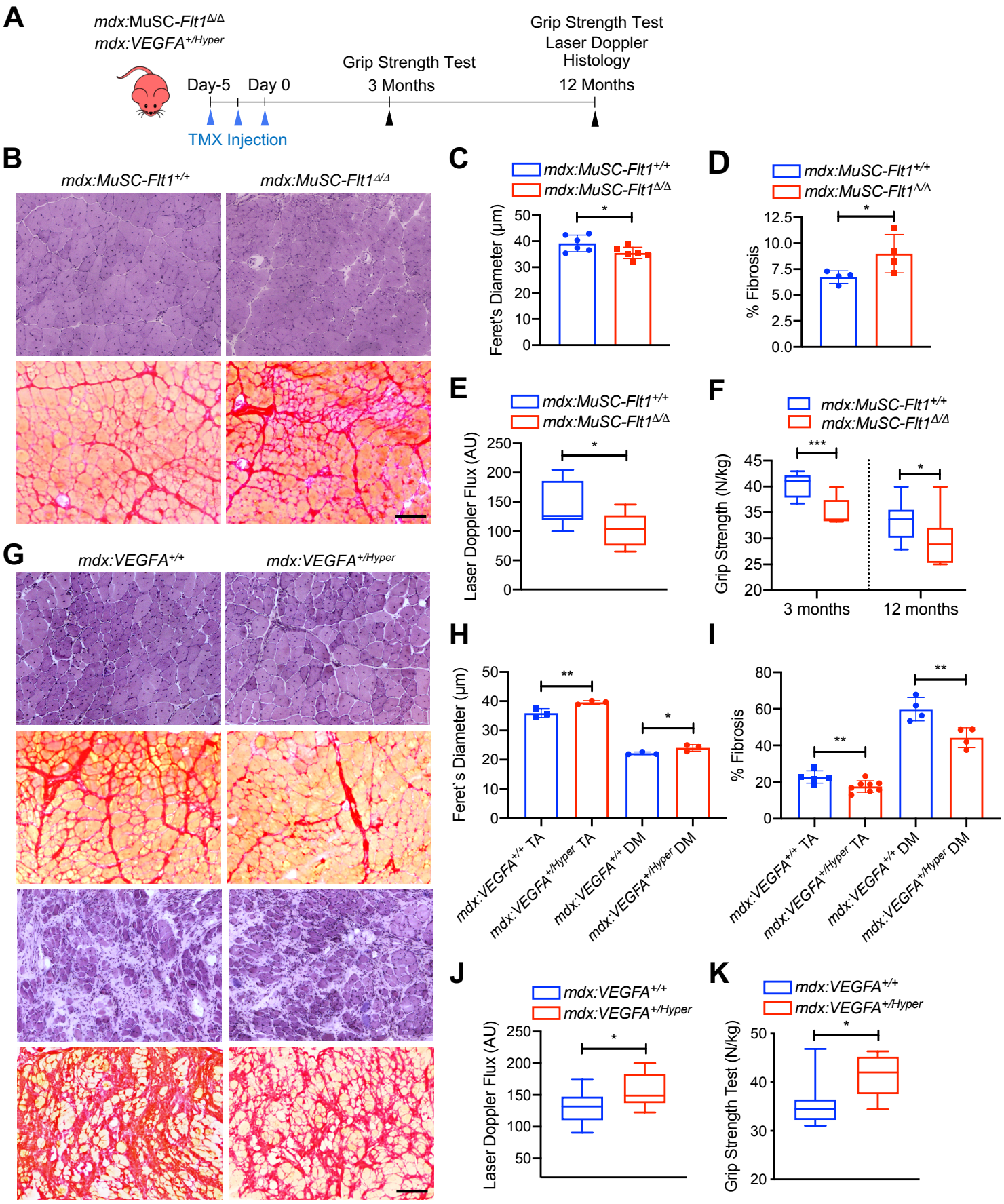
A
mdx:MuSC-Flt1Δ/Δ
mdx:VEGFA+/Hyper
Day-5
Day 0
TMX Injection
Grip Strength Test
3 Months
Grip Strength Test
Laser Doppler
Histology
12 Months
B
mdx:MuSC-Flt1+/+
mdx:MuSC-Flt1Δ/Δ
C
mdx:MuSC-Flt1+/+
mdx:MuSC-Flt1Δ/Δ
Feret's Diameter (µm)
D
mdx:MuSC-Flt1+/+
mdx:MuSC-Flt1Δ/Δ
% Fibrosis
E
mdx:MuSC-Flt1+/+
mdx:MuSC-Flt1Δ/Δ
Laser Doppler Flux (AU)
F
mdx:MuSC-Flt1+/+
mdx:MuSC-Flt1Δ/Δ
Grip Strength (N/kg)
3 months
12 months
G
mdx:VEGFA+/+
mdx:VEGFA+/Hyper
H
Feret's Diameter (µm)
mdx:VEGFA+/+ TA
mdx:VEGFA+/Hyper TA
mdx:VEGFA+/+ DM
mdx:VEGFA+/Hyper DM
I
% Fibrosis
mdx:VEGFA+/+ TA
mdx:VEGFA+/Hyper TA
mdx:VEGFA+/+ DM
mdx:VEGFA+/Hyper DM
J
mdx:VEGFA+/+
mdx:VEGFA+/Hyper
Laser Doppler Flux (AU)
K
mdx:VEGFA+/+
mdx:VEGFA+/Hyper
Grip Strength Test (N/kg)